Live-Cell Imaging of Stress Signaling Dynamics in a Cell Fate Decision

Haruko Miura

Table of contents

List of figures

List of tables

Abstract

Cells in the human body are frequently challenged with a wide range of stresses, including inflammation, oxidative stress, and UV light. In order to adapt to such stresses, multiple signaling pathways have evolved to repair the stress-induced damage or eliminate severely damaged cells through induction of apoptosis. Such crucial cell fate decisions between cell survival and death are, at least in part, mediated by the stress activated protein kinases (SAPKs), c-Jun N-terminal kinase (JNK) and p38. Increasing evidence suggests that crosstalk signaling between JNK and p38 pathways is an important regulatory mechanism in the inflammatory and stress responses. Specifically, suppression of JNK signaling by p38 and its physiological relevance have been documented in cell lines and animal models. However, the effects of this cross-inhibition of JNK by p38 on the precise signaling dynamics, cell-to-cell variation, and cell fate decisions at the single-cell level remain unknown. To address these questions, I established a multiplexed live-cell imaging system based on kinase translocation reporters and simultaneously monitored p38 and JNK activities with high sensitivity and specificity at single-cell resolution. The imaging system enabled visualization of various JNK and p38 activity dynamics in response to different stresses, such as anisomycin, osmotic stress, UV light, and pro-inflammatory cytokines. Under all stress conditions, p38 suppressed JNK activity in a cross-inhibitory manner. Quantitative experimental analysis revealed that p38 antagonized JNK through both post-translational and transcriptional mechanisms, and that the relative strength of these cross-inhibition mechanisms was dependent on the stimulant. Phosphorylation of TGF-β activated kinase 1 binding protein (TAB1) and induction of dual specificity phosphatase 1 (*DUSP1*) were confirmed to be involved in post-translational and transcriptional cross-inhibition of JNK, respectively. Strikingly, inhibition of JNK by p38 reduced the cell-to-cell variation of JNK activity after stress exposure, suggesting that cross-inhibition of JNK by p38 generated cellular heterogeneity in JNK activity. Single cell analysis of endogenous DUSP1 protein levels revealed that the cell-to-cell variation in JNK activity arose from heterogeneous *DUSP1* induction after UV exposure. Strikingly, this heterogeneity in JNK activity was associated with cell survival and death in response to UV stress. These data indicate that cell-to-cell variation in JNK activity leads to fractional killing in response to UV stress.

Chapter 1

Introduction

1-1 Stress activated protein kinases JNK and p38

c-Jun N-terminal kinase (JNK) and p38 are stress-activated protein kinases (SAPKs) that convert a variety of environmental stress and inflammatory signals to diverse cellular functions, such as cell cycle arrest, apoptosis, and inflammatory responses (Cuadrado and Nebreda, 2010; Johnson and Lapadat, 2002; Weston and Davis, 2007) (Figure 1). They belong to the family of mitogen-activated protein kinases (MAPK), which are activated in a three-tiered pathway architecture. MAPK kinase kinases (MAPKKK, MAP3K, MEKK or MKKK) phosphorylate and activate MAPK kinases (MAPKK, MAP2K, MEK or MKK), which in turn phosphorylate and activate MAPKs. Human JNK proteins are encoded by three genes, *MAPK8* (JNK1), *MAPK9* (JNK2), and *MAPK10* (JNK3), of which JNK1 and JNK2 are ubiquitously expressed, while JNK3 is primarily expressed in the brain (Bode and Dong, 2007). Four genes encode human p38 proteins, namely *MAPK14* (p38α), *MAPK11* (p38β), *MAPK12* (p38γ), and *MAPK13* (p38δ). Only p38α is highly expressed in most cell types, while p38β is ubiquitously expressed at very low levels and p38γ/p38δ exhibit tissue-specific expression patterns (Ono and Han, 2000).

JNK proteins are activated by the MKK4 and MKK7 MAPKKs, while p38 is mainly activated by MKK3 and MKK6, but also by MKK4. In contrast to the limited number of MAPKKs, numerous MAPKKKs function upstream of p38 and/or JNK, including MEKK1/2/3/4, apoptosis signal-regulating kinase 1 (ASK1), thousand-and-one amino acids protein kinases 1/2 (TAO 1/2), transforming growth factor β-activated kinase 1 (TAK1), and mixed lineage kinases (MLKs) (Cuevas et al., 2007). These MAPKKKs allow responses to diverse stress signals such as oxidative stress, osmotic shock, ultraviolet (UV) irradiation, DNA damage, heat shock, protein synthesis inhibitors, and pro-inflammatory cytokines (Cuevas et al., 2007).

After activation, SAPKs phosphorylate their target substrates, including protein kinases, regulatory proteins, and various transcription factors, in order to exert their diverse functions (Raman et al., 2007; Wagner and Nebreda, 2009). A major target of JNK is the transcription factor c-Jun (Dérijard et al., 1994; Hibi et al., 1993), but JNK also phosphorylates other transcription factors, such as activating transcription factor 2 (ATF2) (Gupta et al., 1995), Elk-1 (Whitmarsh et al., 1995), p53 (Fuchs et al., 1998), and c-Myc (Noguchi et al., 1999) , as well as cytosolic regulatory proteins such as Bcl-2 and 14-3-3 proteins (Yamamoto et al., 1999; Yoshida et al., 2005). The large number of downstream substrates of JNK allows this pathway to regulate a variety of cellular functions, ranging from

apoptosis induction to enhanced survival and proliferation. The diverse outcomes of JNK signaling were attributed to differences in cell type and stimulus, but also intensity and duration of JNK activation (Bode and Dong, 2007). p38α phosphorylates and activates several protein kinases, including MAPK-activated kinase 2 (MK2) (Rouse et al., 1994), MK3 (McLaughlin et al., 1996), mitogen and stress activated kinase 1 (MSK1) (Deak et al., 1998), MAPK interacting protein kinase 1 (MNK1), and MNK2 (Waskiewicz et al., 1997). p38 also regulates many transcription factors, such as p53 (Bulavin et al., 1999), ATF2 (Raingeaud et al., 1995), Elk-1 (Raingeaud et al., 1996), and myocyte specific enhancer factor 2 (MEF2) (Han et al., 1997; Zhao et al., 1999), and regulatory proteins, such as Cyclin D (Casanovas et al., 2000), Bax (Kim et al., 2006), and BimEL (Cai et al., 2006). The many p38 substrates enable a broad spectrum of cellular responses, including induction of inflammation, apoptosis, and cell cycle arrest (Cuenda and Rousseau, 2007; Ono and Han, 2000).

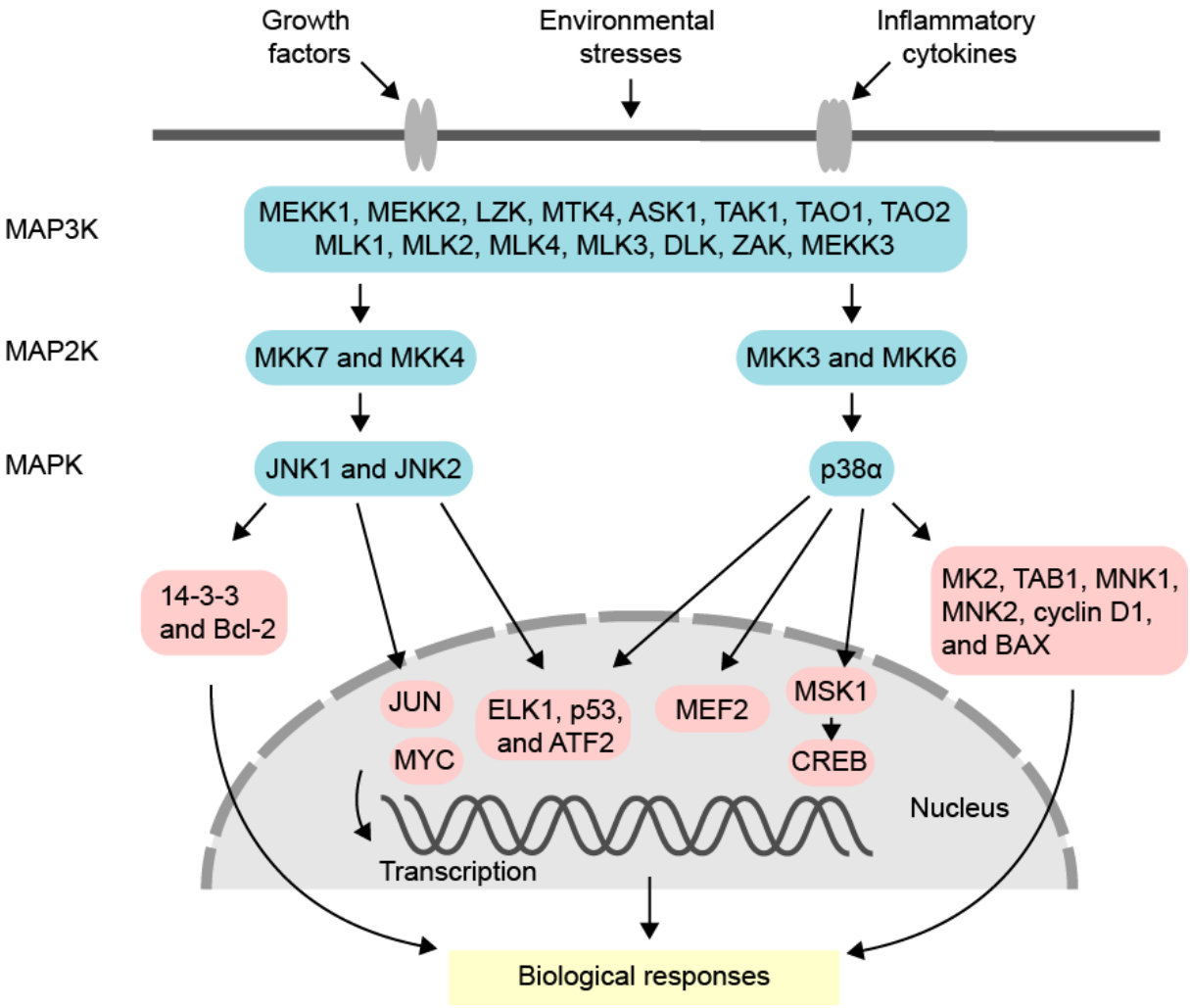

Figure 1. SAPK pathways.

The JNK and p38 pathway are activated by environmental stresses and inflammatory stimuli. The different upstream activators, MAPKKs and MAPKKKs, and downstream substrates are depicted, which lead to a broad range of biological responses.

1-2 Crosstalk of JNK and p38

Crosstalk between the JNK and p38 MAPK pathways is an important regulatory mechanism in the context of both cell lines and animal models. In particular, increasing evidence supports that the p38 pathway can negatively regulate JNK, an example of so-called "cross-inhibition". The first indication for this cross-inhibition is the finding that chemical inhibition and/or knock out (KO) of p38α increased JNK activity in response to pro-inflammatory cytokines and osmotic shock in a epithelial cell line, as well as in mouse embryonic fibroblasts (MEFs) and lipopolysaccharide (LPS)-stimulated macrophages (Cheung et al., 2003). As to the mechanism underlying this cross-inhibition, it has been proposed that p38 inhibits TAK1, a common upstream MAPKKK of p38 and JNK, by phosphorylation of TAK1-binding protein (TAB1) (Cheung et al., 2003) (Figure 2). In support of the role of TAK1 in cross-inhibition, another study has shown that p38α depletion in the intestine and skin caused aberrant activation of TAK1 and JNK after chemically induced inflammation, rendering these tissues more sensitive to inflammation-induced apoptosis than that of the wild type mouse (Caballero-Franco et al., 2013). Mice with liver-specific deletion of the *p38α* gene exhibit increased proliferation of chemically induced liver cancer cells by the enhancement of MKK7-dependent JNK activation (Hui et al., 2007). These mice also exhibit increased JNK and MKK3/6/4 activation by LPS (Heinrichsdorff et al., 2008). Another study reported that JNK activation by p38 inhibitors was dependent on the MAPKKK MLK3 and MKK4/MKK7 in a lung cancer cell line (Muniyappa and Das, 2008). Altogether, p38 suppresses JNK via different MAPKK/MAPKKK in tissue specific manners.

p38α upregulates transcription of dual specificity phosphatase 1 (*DUSP1*) gene, also known as MAPK phosphatase-1 (MKP-1); this transcription product dephosphorylates and inactivates p38 and JNK (Ananieva et al., 2008; Chi et al., 2006; Hammer et al., 2006; Zhao et al., 2006). Mechanistically, p38 activates MSK1, MSK1 then activates the transcription factor cAMP response element-binding protein (CREB), and CREB induces *DUSP1* gene expression (Ananieva et al., 2008; Staples et al., 2010) (Figure 2). For example, myoblasts lacking p38α showed continuous proliferation under differentiation-promoting conditions, and this effect was caused by persistent JNK activation because of a reduction of *DUSP1* expression (Perdiguero et al., 2007). Abrogation of p38α also led to greater JNK

phosphorylation in macrophages and keratinocytes in response to LPS and UV irradiation, respectively, through the reduced induction of *DUSP1* (Kim et al., 2008). Moreover, DUSP1 depletion has been shown to increase JNK activity, and thereby sensitize MEFs to UV-induced apoptosis (Staples et al., 2010). Taken together, these results demonstrate that p38α negatively regulates JNK signaling by different mechanisms, namely, post-translational modification at the level of an upstream MAPKKK and MAPKK and/or transcriptional induction of a JNK-inactivating phosphatase. Notably, these mechanisms are believed to be dependent on the cell types and stimuli (Wagner and Nebreda, 2009). Although the cross-inhibition of JNK by p38 and its physiological relevance have been documented in cell populations by biochemical studies, the degree of cell-to-cell variability and the dynamics of crosstalk between JNK and p38 signaling at the single cell level have not been addressed.

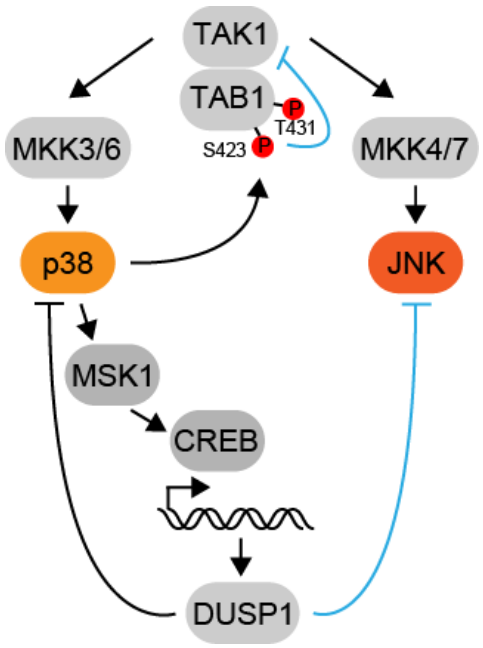

Figure 2. Crosstalk between the p38 and JNK pathway.
p38 phosphorylates TAB1 on Ser423 and Thr431, which leads to inhibition of TAK1 and consequently reduced activation of downstream protein kinases. p38 also induces *DUSP1* gene expression through MSK1 and CREB activation. DUSP1 dephosphorylates and thereby inactivates JNK and p38.

1-3 Cell signaling dynamics in cell fate decisions

Complex signaling networks enable cells to sense environmental signals, process the information, and finally induce specific cell fates to adapt the environmental changes. An increasing number of studies suggests that the dynamic patterns of signaling molecules control cellular responses (Levine et al., 2013; Purvis and Lahav, 2013). Signaling dynamics

are defined as the temporal change in the activity, concentration, localization, or modification state of a signaling molecule. Information can be encoded for example as the amplitude, frequency, duration, onset, rate, or integral of a signaling curve. Researchers in this field have been specifically interested in the following questions: How are signals encoded in dynamic patterns? How are signaling dynamics decoded to cellular phenotypes?

One of the earliest concepts emerging from the study of signaling dynamics is that different upstream signals can lead to different signaling dynamics of the same molecule, which are associated with or at least precede different cell fates (Figure 3A). In a pioneering example, striking difference in the fate of rat neuronal precursor cells was demonstrated upon stimulation by epidermal growth factor (EGF) and nerve growth factor (NGF), both of which signal through the MAPK extracellular signal-regulated kinase (ERK). EGF led to transient activation of ERK and proliferation, while NGF induced sustained ERK activity and differentiation of the cells (Marshall, 1995). In another classic example, different inflammatory stimuli induced distinct activity profiles of the nuclear factor-kappaB (NF-κB) pathway. Tumor necrosis factor α (TNFα) generated oscillations of NF-κB, whereas LPS led to single prolonged activation curve with slower kinetics. These dynamics were accompanied with distinct target gene expression patterns (Werner et al., 2005). Moreover, the tumor suppressor p53 shows stimulus-dependent dynamic behavior, which correlates with different cell fates. DNA damage caused by γ-irradiation leads to a series of repeated p53 pulses and transient cell-cycle arrest. In contrast, DNA damage caused by UV irradiation triggered a single, prolonged pulse of p53 accumulation and apoptosis (Purvis et al., 2012). These examples indicate that signaling dynamics correlate with specific cellular responses and fates. Further elegant perturbation studies using genetic, pharmacological, and optogenetic strategies showed that dynamical patterns not only correlate, but cause certain cellular responses (Aoki et al., 2013; Purvis et al., 2012; Santos et al., 2007).

In earlier studies, temporal signaling patterns had been measured across populations of cells, which in some cases could lead to a misrepresentation of the individual signaling dynamics in the cells. Technical advances in fluorescent probes and live-cell imaging, however, enabled tracking of signaling responses at single-cell resolution. Those technologies uncovered that individual cells can respond heterogeneously to an uniform environmental stimulus. For example, when cells are exposed to cytotoxic agents, some cells undergo apoptosis, while a fraction of cells survives; a phenomenon called fractional killing. Quantitative imaging identified signaling thresholds in cytokine-induced caspase 8 activity or chemotherapy-induced p53 activity, that distinguished surviving from dying cells (Paek et al.,

2016; Roux et al., 2015) (Figure 3B). Such fractional killing can lead to resistance to chemotherapy and is thus a major obstacle to effective cancer treatment. In some cases, specific mutations can allow a subset of cells to survive (Holohan et al., 2013). Analysis of isogenic cells revealed that intrinsic noise and stochastic fluctuations of gene expression can increase cell-to-cell variability of protein abundances, which is known as non-genetic heterogeneity (Brock et al., 2009; Spencer et al., 2009).

In response to environmental stresses, cells might either undergo cell-cycle arrest and seek to repair the stress-induced damage or, if the damage is too severe, undergo senescence or apoptosis. The stress inputs are sensed and transmitted to a number of intracellular signaling cascades and the SAPK and p53 pathways are of particular importance among others. As discussed above, several mechanisms have been proposed for p53 to explain the alternative cell fate decisions in a manner dependent on the signaling dynamics or signaling threshold. However, especially many cancer cells do not harbor functional p53, suggesting that alternative pathways like the SAPKs might be involved in the cell fate decisions between cell survival and death. Measuring the single-cell dynamics of SAPKs will be key to understand how JNK and p38 regulate cell fate decisions.

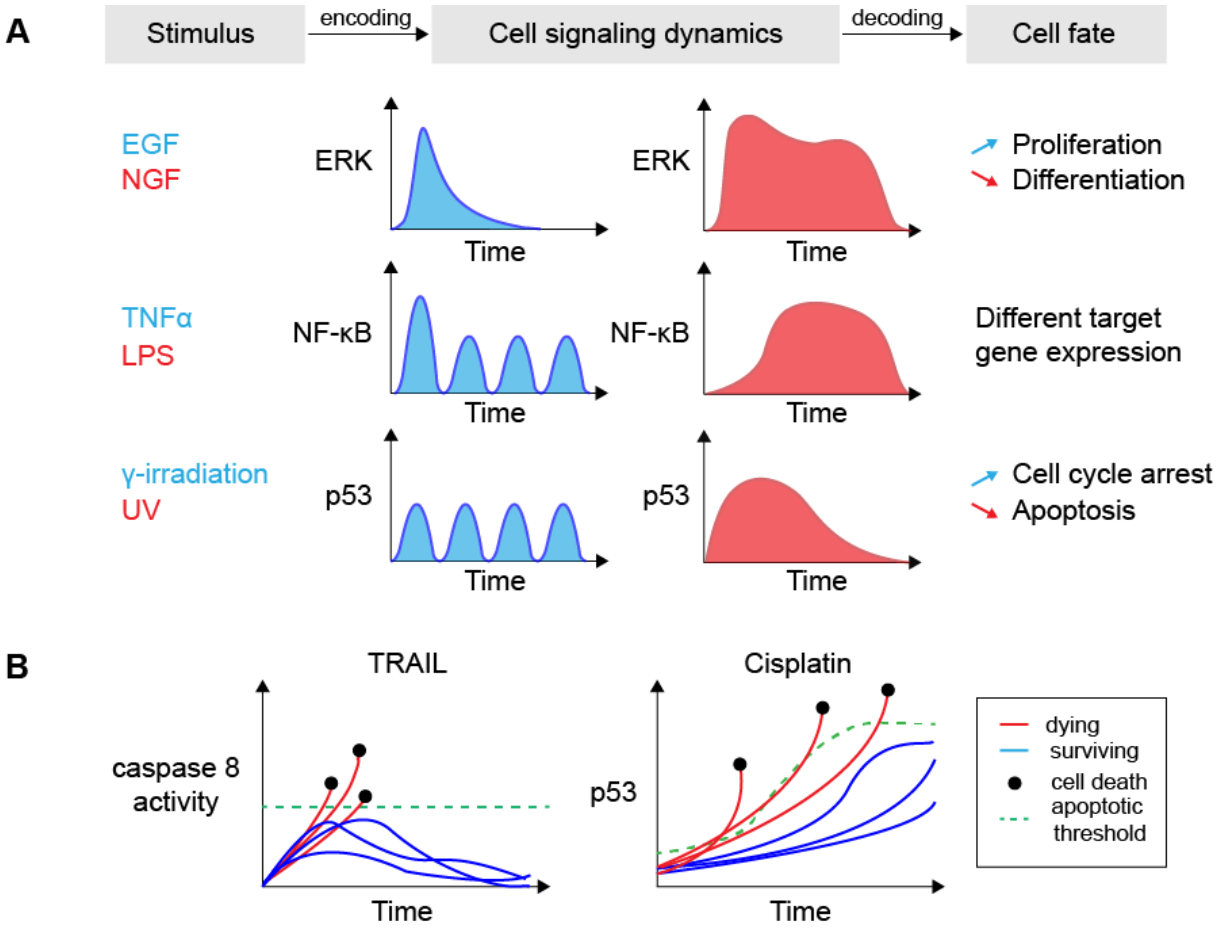

Figure 3. Encoding and decoding of cell signaling dynamics.
(A) Different stimuli induced specific signaling dynamics of key signaling proteins and lead to alternative cell responses.
(B) Signaling thresholds were identified to distinguish between dying and surviving cells.

1-4 Live-cell imaging of protein kinase activities

Understanding the role of signaling dynamics in biological responses requires collection of high-quality time series data at appropriate sampling frequency. Development of fluorescent biosensors and live-cell imaging techniques has immensely improved our ability to quantify and explore the dynamic behavior of signaling molecules in single cells. For monitoring activities of protein kinases (from hereinafter referred to simply as kinase), such as JNK and p38, different types of fluorescent protein (FP)-based reporters have been developed.

To date, Förster resonance energy transfer (FRET) biosensors are the most commonly used tools for monitoring kinase activity in living cells, and, indeed, FRET biosensors for JNK and p38 MAPK are available nowadays (Fosbrink et al., 2010; Komatsu et al., 2011; Tomida et al., 2015). Most genetically-encoded FRET biosensors for kinases consist of a single polypeptide comprising a substrate peptide and a phospho-binding domain (PBD), connected by a flexible linker and flanked by a pair of donor and acceptor FPs, typically a yellow FP (YFP) and cyan FP (CFP) (Komatsu et al., 2011). Phosphorylation of the substrate sequence by the target kinase induces a conformational change due to binding of the PBD to the phosphorylated substrate, resulting in an increase in the FRET efficiency (Figure 4A). FRET biosensors allow measurement of kinase activities specific to subcellular compartments and ratiometric imaging (FRET/CFP ratio) makes these sensors not only robust to small focus drifts and object motions but also independent of expression levels, in comparison to most single-fluorophore kinase reporters (Maryu et al., 2018). For these advantages, FRET biosensors are widely being used for cell biology applications. However, a caveat of the FRET biosensors is that simultaneous imaging of multiple kinase activities is technically challenging with a FRET biosensor, since most FRET biosensors consist of two fluorophores such as YFP and CFP.

To overcome this issue, single-fluorophore kinase translocation reporters (KTRs) provide a powerful alternative by multiplexed imaging using differently colored FPs (Durandau et al., 2015; Li et al., 2017; Maryu et al., 2016; Regot et al., 2014). Upon phosphorylation by the kinases, these reporters translocate from the nucleus to cytosol, and subsequently go back to the nucleus upon de-phosphorylation. Such nucleocytoplasmic shuttling mimic the relocalization of some authentic target proteins of kinases (Hao et al.,

2013; Komeili and O'Shea, 1999; Nardozzi et al., 2010). The prototype KTR is an engineered protein construct in which the kinase docking site of a substrate is fused to a bipartite nuclear localization signal (bNLS) and nuclear export signal (NES), as well as a FP (Regot et al., 2014). The negative charge introduced by phosphorylation inhibits the bNLS and enhances the NES signal, presumably by changing affinities to the nuclear import and export machinery, respectively. Upon phosphorylation, nuclear import and export of the KTR are decreased and increased, respectively, leading to the translocation of the reporter from nucleus to cytosol. Thus, the ratio of cytosolic to nuclear fluorescence intensity (C/N ratio) can be used as a proxy for kinase activity (Regot et al., 2014). The visualization of kinase activity requires only one FP, which can be flexibly swapped with another FP. Multiplexed imaging using translocation reporters is relatively simple, as long as different FPs with minimal spectral overlap are used. For example, KTRs enabled visualization of ERK, JNK, and p38 activities simultaneously in single cells (Regot et al., 2014). Thus, translocation reporter are a powerful tool for analysis of multiple kinase pathways in single cells.

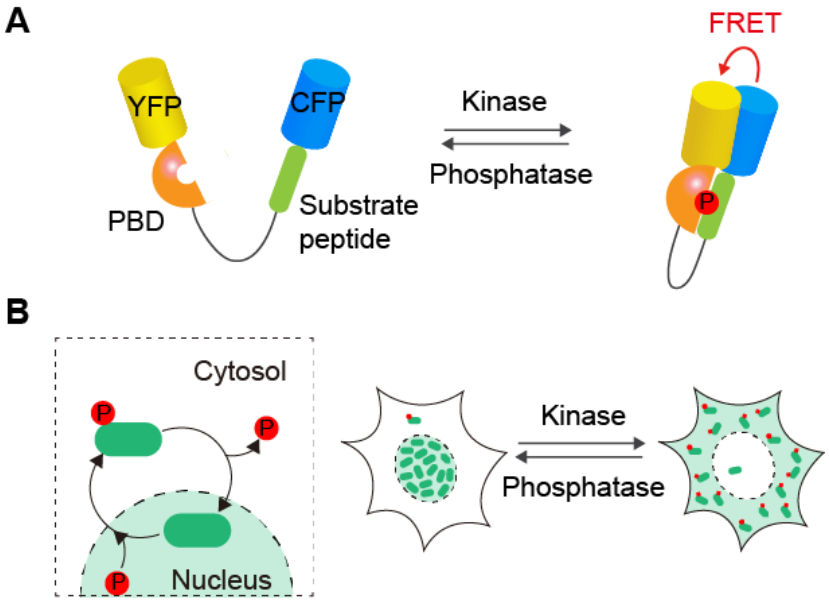

Figure 4. Principles of fluorescence reporters for kinases.
(A) FRET biosensor for kinase activity.
(B) KTR.

1-5 Objective

The SAPKs JNK and p38 are central signaling transmitters in the cellular response to environmental stress and inflammatory signals. An increasing number of studies identified

crosstalk between the JNK and p38 pathways as a critical regulatory mechanism in the stress and inflammatory response in different biological contexts. However, it is still unknown, how this crosstalk affects signaling dynamics, cell-to-cell variation, and cell fates at the single-cell level. In this study, I aim to address these questions by analysis of following objectives:

- Establishment and characterization of a multiplexed imaging system for p38 and JNK activities
- Quantitation of signaling dynamics of p38 and JNK in various stress and inflammatory conditions
- Analysis of crosstalk between p38 and JNK using genetic and pharmacological perturbation
- Analysis of molecular mechanisms underlying the cross-inhibition of JNK by p38
- Analysis of heterogeneity in JNK and p38 activities during stress response in single cells.
- Effect of cell-to-cell variation in SAPK signaling dynamics on cell fate decisions

Chapter 2

Materials and Methods

2-1 Plasmids

Standard molecular biology methods were used for plasmid constructions. To generate pT2Apuro-NLS-iRFP-NLS, the NLS of SV40 large T antigen (PKKKRKV) was attached to the 5' and 3' end of iRFP by PCR and this fragment was inserted into the pT2Apuro vector (Kawakami and Noda, 2004). The pT2Apuro vector is a Tol2 transposon vector with IRES-pac (puromycin resistance gene) and was kindly gifted from Dr. K. Kawakami (National Institute for Genetics, Japan). The JNK KTR sequence was obtained by PCR from pLentiPGK Puro DEST JNKKTRClover (Regot et al., 2014), a kind gift from Dr. M. Covert (Addgene plasmid #59151). JNK KTR and mCherry were then cloned into pCAGGS (Niwa et al., 1991), an eukaryotic expression vector, or pPBbsr, a piggyBac transposon vector with IRES-bsr (blasticidin S resistance gene) (Yusa et al., 2009), producing pCAGGS-JNK KTR-mCherry and pPBbsr-JNK KTR-mCherry. The pPB backbone was obtained as a kind gift from Dr. A. Bradley (Wellcome Trust Sanger Institute, UK). p38 KTR (Regot et al., 2014) was generated by PCR from annealed sense- and antisense Oligo DNAs and inserted into a pPBbsr-mEGFP vector, resulting in pPBbsr-p38 KTR-mEGFP. For construction of pPBbsr-mEGFP-MK2, pCAGGS-mKO-MK2, and pPBbsr-mKO-MK2, the cDNA of human MAPKAPK2 was retrieved from a HeLa cDNA library by PCR and cloned into the pPBbsr or pCAGGS vectors along with mEGFP or mKO. To ease transfection of following three reporters, a polycistronic vector encoding NLS-iRFP-NLS, JNK KTR-mCherry, and mKO-MK2 was constructed. To do so, the reporters were connected by sequences for the self-cleaving P2A peptide (GSGATNFSLLKQAGDVEENPGP) by PCR, and the polycistronic cassette was cloned into the pPBbsr vector. This vector was named pNJP (Nuclear, JNK, and p38 reporter). I amplified the cDNA of human TAB1 from HeLa cDNA by PCR and introduced the S423A and T431A point mutations by two-step overlap-extension PCR. The cDNAs of TAB1 wildtype and SATA were cloned into the lentiviral vector pCSIIneo vector with IRES-neo (neomycin resistance gene), to obtain pCSIIneo-TAB1-wt and pCSIIneo-TAB1-SATA. The CSII-EF lentiviral vector was a kind gift from Dr. H. Miyoshi (RIKEN, Japan).To construct the caspase 3 FRET biosensor EC-RP (Albeck et al., 2008), annealed Oligo DNAs for the caspase 3 substrate site (SGLRSSGDEVDRVYGSGS) were cloned between the FPs of pPBbsr2-YPet-SECFP-NES (Komatsu et al., 2011) by linker ligation, producing the vector pPBbsr-EC-RP-NES. pX459 (pSpCas9(BB)-2A-Puro) and lentiCRISPR v2 were kind gifts from Dr. F. Zhang (Addgene plasmids #48139 and #52961) (Ran et al., 2013; Sanjana et al., 2014).

Table 1. List of plasmids.

Plasmid name	Source	Identifier
pT2Apuro-NLS-iRFP-NLS	This study	N/A
pLentiPGK Puro DEST JNKKTRClover	Regot et al., 2014	addgene #59151
pCAGGS-JNK KTR-mCherry	This study	N/A
pPBbsr-JNK KTR-mCherry	This study	N/A
pPBbsr-p38 KTR-mEGFP	This study	N/A
pPBbsr-mEGFP-MK2	This study	N/A
pCAGGS-mKO-MK2	This study	N/A
pPBbsr-mKO-MK2	This study	N/A
pNJP	This study	N/A
pCSIIneo-TAB1-wt	This study	N/A
pCSIIneo-TAB1-SATA	This study	N/A
pT2Apuro-IC-RP-NES	This study	N/A
pPBbsr-EC-RP-NES	This study	N/A
perky p38 NES	Tomida et al., 2015	N/A
lentiCRISPRv2-hMAPK14	This study	N/A
lentiCRISPRv2-hMAPK8	This study	N/A
lentiCRISPRv2-hMAPK9	This study	N/A
lentiCRISPRv2-hTAB1	This study	N/A
lentiCRISPRv2-hMAP3K7	This study	N/A
lentiCRISPRv2-hDUSP1	This study	N/A
lentiCRISPRv2-RLuc8	Aoki et al. 2017	N/A
pX459-hDUSP1-3'end	This study	N/A
pCAGGS-mScarlet-loxP-P2A-dTKneo-pA-loxP-stop	This study	N/A
pCAGGS-T2TP	Kawakami and Noda, 2014	N/A

pCMV-mPBase(neo-)	Yusa et al., 2009	N/A
psPAX2	Didier Trono lab (unpublished)	addgene #12260
pCMV-VSV-G-RSV-Rev	Miyoshi et al., 1998	N/A

2-2 Reagents

Reagents and antibodies were purchased from following sources (Table 2).

Table 2. List of reagents.

Reagent	Source	Identifier
Chemicals, peptides, and recombinant proteins		
Actinomycin D	Sigma Aldrich	A1410
Anisomycin	Sigma Aldrich	A9789
BIRB 796	Calbiochem	506172
Blasticidin S	InvivoGen	ant-bl-1
DMSO	Nacalai Tesque	13445-74
G418	InvivoGen	ant-gn-5
IL-1β (recombinant, human)	R&D Systems	201-LB-005
JNK inhibitor VIII	Cayman Chemical	15946
Puromycin	InvivoGen	ant-pr-1
SB203580	Selleck Chemicals	S1076
Sorbitol	Wako	198-03755
TNFα (recombinant, human)	R&D Systems	210-TA-005
VX-745	Adipogen	SYN-1123-M001
Antibodies		
Anti-mCherry antibody	Abcam	ab167453
Anti-monomeric Kusabira Orange 2 pAb	MBL	PM051M

Anti-RFP mAb	MBL	M204-3
SAPK/JNK Antibody	Cell Signaling Technology	#9252
Phospho-SAPK/JNK (Thr183/Tyr185) (G9) Mouse mAb	Cell Signaling Technology	#9255
JNK1 (2C6) Mouse mAb	Cell Signaling Technology	#3708
JNK2 (56G8) Rabbit mAb	Cell Signaling Technology	#9258
p38 MAPK Antibody	Cell Signaling Technology	#9212
Phospho-p38 MAPK (Thr180/Tyr182) (28B10) Mouse mAb	Cell Signaling Technology	#9216
TAB1 (C25E9) Rabbit mAb	Cell Signaling Technology	#3226
TAK1 (D94D7) Rabbit mAb	Cell Signaling Technology	#5206
αTubulin Antibody (DM1A)	Santa Cruz	sc-32293
Anti-α-Tubulin pAb	MBL	PM054
IRDye 680LT goat anti-rabbit IgG	LI-COR Biosciences	925-68021
IRDye 800CW donkey anti-mouse IgG	LI-COR Biosciences	925-32212

2-3 Maintenance of cell lines

HeLa cells were obtained from the Human Science Research Resources Bank (Japan). MCF10A and A549 cells were purchased from American Type Culture Collection. NIH3T3 cells were a gift from Dr. J. Nakayama (National Institute for Basic Biology, Japan). MCF10A cells were kept in DMEM/F12 (Invitrogen) supplemented with 5% horse serum (Invitrogen), 20 ng/ml epidermal growth factor (Nacalai), 100 ng/ml cholera toxin (List Biological Laboratories), 10 μg/ml insulin (Nacalai), 0.5 mg/ml hydrocortisone (Nacalai), 100 u/ml penicillin/100 μg/ml streptomycin (Nacalai). A549, NIH3T3, and HeLa cells were cultured in Dulbecco's Modified Eagle's Medium (DMEM) high glucose (Wako; Nacalai) supplemented with 10% fetal bovine serum (FBS) (Sigma Aldrich). Antibiotics were added, if required.

2-4 Transient and stable expression

A transient expression system was established by transfection of HeLa cells with pCAGGS vectors using 293fectin (Invitrogen) according to the manufacturer's protocols. On the other hand, to establish stable cell lines expressing the fluorescent reporters, Tol2- and piggyBac-transposon based systems were applied. The transposase encoding pCAGGS-T2TP vector (a kind gift of Dr. K. Kawakami, National Institute for Genetics, Japan) and pCMV-mPBase (neo-) vector (a kind gift of Dr. A. Bradley, Wellcome Trust Sanger Institute, UK) were co-transfected with the reporters encoding pT2Apuro and pPBbsr vectors, respectively, using 293fectin. One day after transfection, cells were selected with 1 μg/ml puromycin or 20 μg/ml blasticidin S for at least one week. The reporter HeLa cell line expressing NLS-iRFP-NLS, JNK KTR-mCherry, and mKO-MK2 simultaneously, were generated by introducing the piggyBac and Tol2 transposon system. Subsequently, clonal cell lines were isolated by single-cell cloning and screened for iRFP, mCherry, and mKO expression. Moreover, to ease generation of cell lines expressing the three reporters, the piggyBac transposon system was applied to stably transfect the polycistronic vector pNJP. However, it is worth to mention that the expression levels of the polycistronic construct were reduced in comparison to the reporters when they were individually expressed. For generation of other cell lines stably expressing NJP using the piggyBac transposon system, Lipofectamine 3000 Reagent (Thermo Fisher Scientific) was used to transfect NIH3T3 and A549 cells. MCF10A cells were transfected by Viromer RED (Lipocalyx). For functional analysis of TAB1 protein, HeLa TAB1 KO cells were complemented with the wild-type or mutant TAB1, using lentivirus-mediated gene transfer system. Concisely, the lentiviral pCSIIneo vector was transfected into Lenti-X 293T cells (Clontech) along with the packaging plasmid psPAX2 (a gift from Dr. D. Trono -Addgene plasmid #12260), and pCMV-VSV-G-RSV-Rev (a kind gift of Dr. Miyoshi, RIKEN, Japan) by using the linear polyethyleneimine "Max" MW 40,000 (Polyscience). Target cells were infected with the virus-containing media after two days. The cells were selected beginning at two days after infection, by at least one week of treatment with 1 mg/ml G418. All cells were kept at 37 ˚C in a humidified atmosphere of 5% CO_2.

2-5 CRISPR/Cas9-mediated KO

For KO of human *DUSP1*, *MAPK8*, *MAPK9*, *MAPK14*, *MAP3K7*, and *TAB1* genes by the clustered regularly interspaced short palindromic repeats (CRISPR)/CRISPR-associated

protein-9 nuclease (Cas9) system, I designed custom single guide RNAs (sgRNA) sequences targeting the start codon or first exon using the CRISPR Design online tool (http://crispr.mit.edu, Zhang Lab, MIT). The TAB1 sgRNA is homologous to a sequence upstream of the start codon, enabling exogenous expression of TAB1 in *TAB1* KO cells, although they stably express the sgRNA and Cas9. The sgRNA targeting sequences are given in Table 3. Oligo DNAs for the sgRNAs were annealed and inserted into the lentiCRISPR v2 vector that was digested with *Bsm*BI restriction enzyme (Addgene plasmid #52961) (Sanjana et al., 2014). Lentiviral gene transfer was used to introduce the sgRNA/Cas9 cassette into HeLa cells. After selection of infected cells by 2 μg/ml puromycin for at least two days, cells were subjected to single-cell cloning. Western blotting confirmed depletion of target proteins. Since specific antibodies for DUSP1 were not available, *DUSP1* KO was validated by sequencing and indel analysis using the TIDE webtool (https://tide-calculator.nki.nl/) (Brinkman et al., 2014).

Table 3. Targeting sequences for CRISPR/Cas9 mediated gene KO.

Target	targeting sequence
hDUSP1	CTACTAACCTGATCGTAGAG
hMAPK8	ACGCTTGCTTCTGCTCATGA
hMAPK9	TCAGTTTTATAGTGTGCAAG
hMAPK14	AGCTCCTGCCGGTAGAACGT
hMAP3K7	CATCTCACCGGCCGAAGACG
hTAB1	CCTCCTCTGCGCCGCCATCT
RLuc8	AGGTGTACGACCCCGAGCAG

2-6 CRISPR/Cas9-mediated knock-in

A previously described protocol was used to establish a HeLa DUSP1-mScarlet knock-in (KI) cell line (Komatsubara et al., 2017). The sgRNA target sequence was designed to overlap the stop codon of the DUSP1 gene (CCCGTGGCCTTTCAGCAGCT), so that this sgRNA does not recognize the sequence after KI. Annealed Oligo DNA for the sgRNA was inserted into the *Bpi*I digested pX459 vector, generating pX459-hDUSP1-3'end. The donor vector pCAGGS-mScarlet-loxP-P2A-dTKneo-pA-loxP-stop comprised mScarlet, loxP, P2A,

a fusion of truncated herpes simplex virus type 1 thymidine kinase (dTK) and bacterial neomycin phosphotransferase (neo) (dTKneo), a poly(A) signal, and loxP. Linear double stranded (ds) donor DNA template with 40 bp left and right homology arms (40 bp upstream/downstream of the DUSP1 stop codon) was amplified by PCR. HeLa cells were plated on a 35 mm dish and transfected with 50 ng of the dsDNA donor and 1 µg pX459-hDUSP1-3'end by using 293fectin. One day after transfection, cells positive for pX459-hDUSP1-3'end were selected by 1 µg/ml puromycin for 2 days. Afterwards, cells were treated with 500 µg/ml G418 to select of knock-in cells for 10 days. Then, clonal cell lines were isolated by limiting dilution method in presence of 500 µg/ml G418. To remove the loxP flanked P2A-dTKneo-poly(A) selection cassette by recombination, knock-in cells were infected with adeno-associated virus expressing Cre recombinase (AAV-Cre). To produce AAV, LentiX 293T cells were co-transfected with pAAV-Cre, pAAV-DJ, and pHelper and after 3 days cells collected and resuspended in 1 mL DMEM medium. AAV was extracted by four freeze-thaw cycles and removal of cell debris by centrifugation. At least five days after infection, cells were selected with 50 µM Ganciclovir for further 5 days. Genomic DNA of KI cells before and after AAV-Cre infection was extracted with QuickExtract DNA Extraction Solution (Epicentre) and analyzed by PCR. Correct KI of mScarlet was further validated by DNA sequencing and Western blotting.

2-7 RNA isolation and quantitative PCR analysis

Total RNA was extracted by using QIAshredder Kit (QIAGEN) and RNeasy Plus Mini Kit (QIAGEN), following the manufacturer's instructions. After quantification of total RNA amount, reverse transcription was performed using the High-Capacity cDNA Reverse Transcription Kit (Thermo Fisher Scientific), followed by quantitative PCR analyses using the THUNDERBIRD SYBR qPCR Mix (TOYOBO) or Power SYBR Green PCR Master Mix (Thermo Fisher Scientific). Measurements were conducted on an Applied Biosystems StepOne Real-Time PCR System (Thermo Fisher Scientific). The ΔΔCt method was applied for normalization to the housekeeping gene GAPDH and representation of data as fold changes compared to control samples (Schmittgen and Livak, 2008). Following primer sequences were used: DUSP1 Fw: ACCACCACCGTGTTCAACTTC; DUSP1 Rv: TGGGAGAGGTCGTAATGGGG; GAPDH Fw: GAGTCCACTGGCGTCTTCAC; GAPDH Rv: GTTCACACCCATGACGAACA.

2-8 Western Blotting

HeLa cells grown on 6-well or 12-well plates were starved in DMEM medium or FluoroBrite DMEM (Life Technologies) supplemented with 1x GlutaMax (Life Technologies) and 0.2% FBS for at least 3 h and treated with inhibitors and stimulants, when indicated. Cells were lysed in 100 to 300 µl of 1x sodium dodecyl sulphate (SDS) sample buffer (62.5 mM Tris-HCl pH 6.8, 12% glycerol, 2% SDS, 0.004% Bromo Phenol Blue, and 5% 2-mercaptoethanol). After sonication using the ultrasonic wave disruption system Bioruptor II (Cosmo Bio), the samples were separated by SDS-polyacrylamide gel electrophoresis using 13-well or 17-well Extra PAGE One Precast 5- 20% gradient gels (Nacalai) and transferred to Immobilon-FL polyvinylidene fluoride membranes with 0.45 µm pore size (Millipore) using a wet transfer system (Biorad). Membranes were blocked with Odyssey blocking buffer (LI-COR) or skim milk for 1 h and then subsequently incubated with primary antibodies diluted in Odyssey blocking buffer or TBS Tween-20 overnight. Subsequently, membranes were incubated with IRDye680LT- and IRDye800CW-conjugated secondary antibodies (LI-COR) diluted in Odyssey blocking buffer. Two-channel infrared fluorescence detection (700 nm and 800 nm) was conducted by an Odyssey Infrared imaging system (LI-COR) or Odyssey CLx imaging system (LI-COR). Fluorescent signals were analyzed by the Odyssey imaging softwares, Odyssey V3.0 or Image Studio Ver 5.2.

2-9 UV-C irradiation

Cells were irradiated with UV-C light (254 nm) using a CL-100 Ultraviolet Crosslinker (UVP). Just before irradiation most of the medium (4/5th of volume) is removed and cells are left in minimal medium (1/5th of volume), in order they do not dry out. The same culture medium was added back to cells, directly after UV irradiation.

2-10 Apoptosis assay

Apoptosis was quantified by caspase 3 activation by using the FRET biosensor effector caspase reporter protein (EC-RP), which is specifically cleaved by effector caspases (Albeck et al., 2008). EC-RP comprises YPet, a caspase 3 substrate (SGLRSSGDEVDRVYGSGS), SECFP, and NES. The intact reporter shows a high FRET/CFP ratio, while cleavage of the reporter by active caspase 3 leads to a drop in the FRET/CFP ratio. A HeLa cell line stably expressing EC-RP was established by the piggyBac system. These cells were plated to four-

compartment CellView cell culture dishes (Greiner Bio-One) with 3 x 10^4 cells per well in 500 µl medium. The following day, cells were starved for at least 3 h in FluoroBrite DMEM supplemented with 1x GlutaMax and 0.2% FBS, pretreated with inhibitor for about 15 min, and irradiated with UV-C, when indicated. 12 h after UV-C stimulation, EC-RP fluorescence was measured by an IX81 inverted microscope using a 20x objective lens, as described earlier. CFP and FRET images were acquired in 4 to 5 positions per condition. The background was corrected by subtraction of a minimum projection image, the intensities of both the CFP and FRET channels were measured in single cells and exported to Excel Software (Microsoft Corporation) to calculate the FRET/CFP ratio. At least 2000 cells per condition from at least 3 independent experiments were analyzed. EC-RP FRET/CFP ratios showed a bimodal distribution. Cells with a low FRET/CFP ratio (≤ 2) were defined as apoptotic. Time-lapse imaging verified that apoptotic cells did not detach from the glass bottom dish during 12 hours after UV exposure.

2-11 Live-cell imaging

Stable cell lines were imaged, unless otherwise indicated. Cells were seeded to four-compartment CellView cell culture dishes (Greiner Bio-One) or 35 mm glass-bottom dishes (Asahi Techno Glass) and cultured for at least 24 h. Before imaging, the culture medium was replaced with FluoroBrite DMEM supplemented with 1x GlutaMax and 0.2% FBS for at least 3 h and cells were pretreated with inhibitors for about 15 min, if applicable. UV irradiation was performed just before image acquisition, while other stimuli were added after start of imaging. For long-term time-lapse imaging (48 hours), cells were kept in FluoroBrite DMEM supplemented with 1x GlutaMax and 5% FBS. Fluorescence imaging was performed in a 37 ˚C and 5% CO_2 environment with an IX81 inverted microscope (Olympus), equipped with a Spectra-X light engine illumination system (Lumencor), a MAC5000 controller for filter wheels, a UPlanSApo 60x/1.35 oil objective lens (Olympus), an IX2-ZDC laser-based autofocusing system (Olympus), XY stage (Ludl Electronic Products), an incubation chamber (Tokai Hit), a GM-4000 CO2 supplier (Tokai Hit), and a Retiga 4000R cooled Mono CCD camera (QImaging). Long-term imaging was also conducted with an IX83 inverted microscope (Olympus), equipped with a Spectra-X light engine illumination system (Lumencor), a U-CBF control box for filter wheels (Olympus), UPlanSApo 20x/0.75 and

UPlanSApo 40x2/0.75 dry objective lenses (Olympus), an IX3-ZDC2 laser-based autofocusing system (Olympus), IX3-SSU ultrasonic stage (Olympus), an IX3WX incubation chamber (Tokai Hit), an STX Stage Top Incubator (Tokai Hit), and a Prime sCMOS camera (Photometrix). Dichroic mirrors, excitation, and emission filters are listed in Table 4. MetaMorph software (Molecular Devices) was used to operate the microscope.

Table 4. Dichroic mirrors and filter sets.

FP	Lumencor illumination	Excitation filter	Dichroic mirror	Emission filter
IX81				
mKO	Green 549/15	FF01-543/3 (Semrock)	20/80 beamsplitter (Chroma)	FF01-563/9 (Semrock)
mCherry	Green 549/15	FF01-580/20 (Semrock)	20/80 beamsplitter (Chroma)	FF01-641/75 (Semrock)
iRFP	Red 632/22	open	FF408/504/581/667/ 762-Di01 (Semrock)	FF01-692/LP (Semrock)
mScarlet	Green 549/15	FF01-580/20 (Semrock)	86006bs (Chroma)	FF01-641/75 (Semrock)
Clover	Cyan 475/28	open	86006bs (Chroma)	FF01-542/27 (Semrock)
FRET	Blue 438/24	open	XF2034 455DRLP (Omega Optical)	FF01-542/27 (Semrock)
CFP	Blue 438/24	open	XF2034 455DRLP (Omega Optical)	FF01-483/32 (Semrock)
IX83				
mKO	Green 549/15	FF01-543/3 (Semrock)	BK7 glass (EKSMA Optics) or FF409/493/573/652/ 759-Di01 (Semrock)	FF01-563/9 (Semrock)
mCherry	Green 549/15	FF01-575/15 (Semrock)		FF01-641/75 (Semrock)
iRFP	Red 632/22	open		BLP01-664R (Semrock)

2-12 Image analysis

Image analysis was conducted in the MetaMorph software, basically as previously reported (Maryu et al., 2016). For background correction, blank positions (medium only) or minimum planes were subtracted, in order to flat-field the images. To determine the cross-excitation and bleed-through, HeLa cells expressing only one reporter were imaged in each fluorescent channel. If necessary, bleed-through was corrected by subtraction. It should be noted, that for each microscope setting, the cross-excitation and bleedthrough need to be remeasured. For C/N ratio analysis, nuclear and cytosolic regions of interest were placed in single cells and the average fluorescence intensities were extracted. The C/N ratio was calculated as the quotient of cytosolic and nuclear fluorescence intensities using Excel software.

2-13 Quantification of signaling activities

The strength of signaling activities and cross-inhibition in Figure 14D was determined as in the following section: First, the stimulation-to-JNK edge activities were retrieved from the JNK KTR-mCherry C/N ratios in the presence of SB203580 for each stimulation at the indicated time point. Likewise, each stimulation-to-p38 edge activity was picked up from the mKO-MK2 C/N ratio at the indicated time point of the DMSO control. Next, each transcriptional cross-inhibition activity by p38 was determined by subtraction of the JNK KTR-mCherry C/N ratio of the DMSO control from the JNK KTR-mCherry C/N ratio of the actinomycin D condition at the indicated time point. Finally, each post-translational cross-inhibition activity by p38 was quantified by subtraction of the JNK KTR-mCherry C/N ratio of the actinomycin D condition from JNK KTR-mCherry C/N ratio of the SB203580 condition at the indicated time point.

2-14 Regression analysis

Solver functions of Microsoft Excel were used for non-linear regression of dose responses. Concisely, experimental data were fitted with the Hill function to extract EC50 and nH values. Logistic regression analysis was conducted by using Python with the scikit-learn library.

2-15 Statistical analysis

Statistical analysis was performed in Microsoft Excel software. To compare two sets of data, a two tailed, unpaired Student's t-test was used based on the result of the F-test. The F-Test tests the null hypothesis that the variances of two populations are equal. For the Student's t-test, p-values < 0.05 were considered significant, with following levels: $*p < 0.05$, $**p < 0.01$, $***p < 0.001$.

Chapter 3

Results

3-1 A multiplexed imaging system for p38 and JNK activities

To visualize the activities of p38 and JNK simultaneously at the single cell resolution, the first aim was to establish a multiplexed imaging system based on genetically-encoded, single fluorophore, translocation reporters. I first used the previously reported JNK KTR and p38 KTR, which convert phosphorylation signals into nucleo-cytoplasmic shuttling events (Regot et al., 2014). The cytoplasmic to nuclear fluorescence intensity ratio (C/N ratio) of a KTR serves as quantitative read-out of the target kinase activity. The KTR reporters were stably expressed in HeLa cells and their response to the protein synthesis inhibitor anisomycin was monitored, which is a potent activator of JNK and p38 pathways. JNK KTR showed robust translocation from the nucleus to cytosol (shown in later figures), however, p38 KTR exhibited poor cytosolic translocation (Figure 5A).

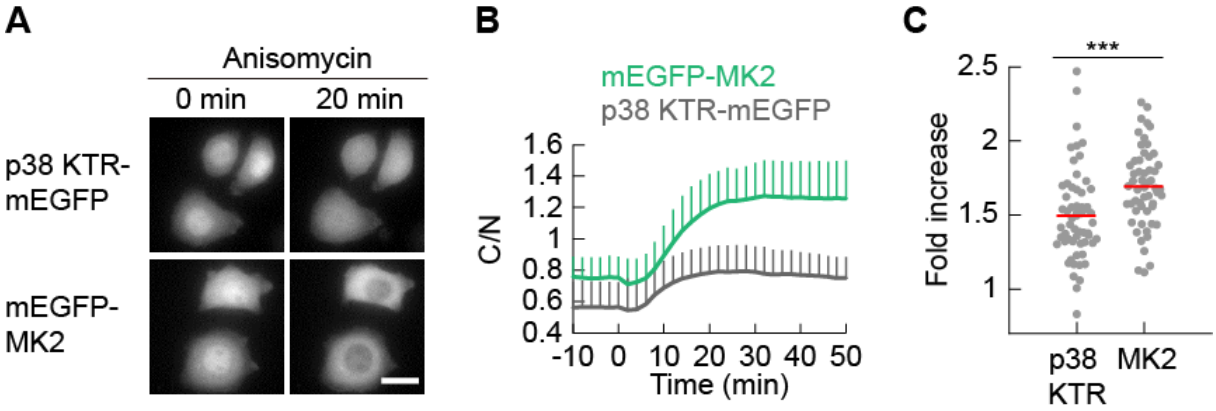

Figure 5. Comparisons of KTRs for p38 kinase activity.
(A) HeLa p38 KTR-mEGFP and mEGFP-MK2 cells were stimulated with 1 μg/ml anisomycin. Representative images are shown. Scale bar: 20 μm.
(B) Mean mEGFP-MK2 and p38 KTR-mEGFP C/N ratios with SD are shown for cells from (A). n = 38 cells for p38 KTR-mEGFP, n = 34 cells for mEGFP-MK2 from two independent experiments.
(C) The fold increases in the p38 KTR-mEGFP and mEGFP-MK2 C/N ratios after 30 min of 1 μg/ml anisomycin treatment are shown for single cells from (A) and as mean (red line). n ≥ 50 cells for each condition from two independent experiments. Significance was tested by a Student's *t*-test. ***p<0.001.

This prompted me to develop an improved translocation-based reporter for p38 activity. Fortunately, the p38α substrate MAPKAPK2 (MK2) naturally redistributes between the nucleus and cytosol, in a manner dependent on the phosphorylation status (Anton et al., 2014; Engel et al., 1998; Meng et al., 2002; Trask et al., 2006). MK2 contains a constitutively accessible NLS and stress-regulated NES sequence in the C-terminal regulatory domain. Activation of MK2 by phosphorylation on Thr222 and Thr334 de-masks the NES, leading to its nuclear export (Engel et al., 1998; Gaestel, 2006). Therefore, I tested MK2 as a live-cell

imaging reporter for p38 activity. Strikingly, mEGFP-MK2, comprising monomeric EGFP (mEGFP) and full-length MK2, surpassed p38 KTR-mEGFP in terms of the C/N ratio increase in response to anisomycin (Figures 5B and 5C). These data suggest, that the MK2-based reporter monitors p38 activity with higher sensitivity than the previously reported p38 KTR. Henceforward, the MK2-based probe was used for imaging of p38 activity.

For co-visualization of JNK and p38 activities, JNK KTR was fused to mCherry and MK2 to monomeric Kusabira Orange (mKO). Furthermore, an NLS flanked near-infrared FP (iRFP) was used as a nuclear marker (Figure 6A). Use of FPs in the red color range not only allows combination with CFP/YFP-based FRET biosensors and optogenetic tools of blue light range, but also reduces phototoxicity to cells. To examine possible cross-excitation and/or bleed-through, I imaged HeLa cells expressing each reporter with all combinations of detection channels and determined their relative contribution to the fluorescence (Figure 6B). The bleed-through and cross-excitation of JNK KTR-mCherry, mKO-MK2, and NLS-iRFP-NLS were minimal with the here applied microscope settings (Figure 6B), allowing multiplexed imaging of these reporters without linear unmixing.

For the following imaging experiments, I established a HeLa cell line stably expressing each of the three reporters by transposon-mediated gene transfer and single-cell cloning, hereinafter referred to as clonal HeLa reporter cells. Anisomycin stimulation induced translocation of JNK KTR-mCherry and mKO-MK2 from the nucleus to cytosol (Figure 6C), which was quantified as the C/N ratio in single cells (Figure 6D). The mKO-MK2 and JNK KTR-mCherry C/N ratios began to rise about 5 and 10 min after addition of anisomycin and reached maximal levels about 20 and 30 min after stimulation, respectively (Fig. 6D).

To study the effect of reporter concentration on the C/N ratio, JNK KTR-mCherry and mKO-MK2 were transiently overexpressed in HeLa cells. For both reporters, the increase in the C/N ratios upon anisomycin stimulation inversely correlated with the expression levels (Figure 6E, left), suggesting that high expression level of the reporters may impede visualization of the translocation, probably because of the existence of a rate-limiting step in nuclear import/export. Meanwhile, in the range of stable expression, the C/N ratio was independent of the reporter expression levels (Figure 6E, right). To minimize the effect of reporter concentrations on the output, we thus established stable cell lines for all experiments using KTR reporters.

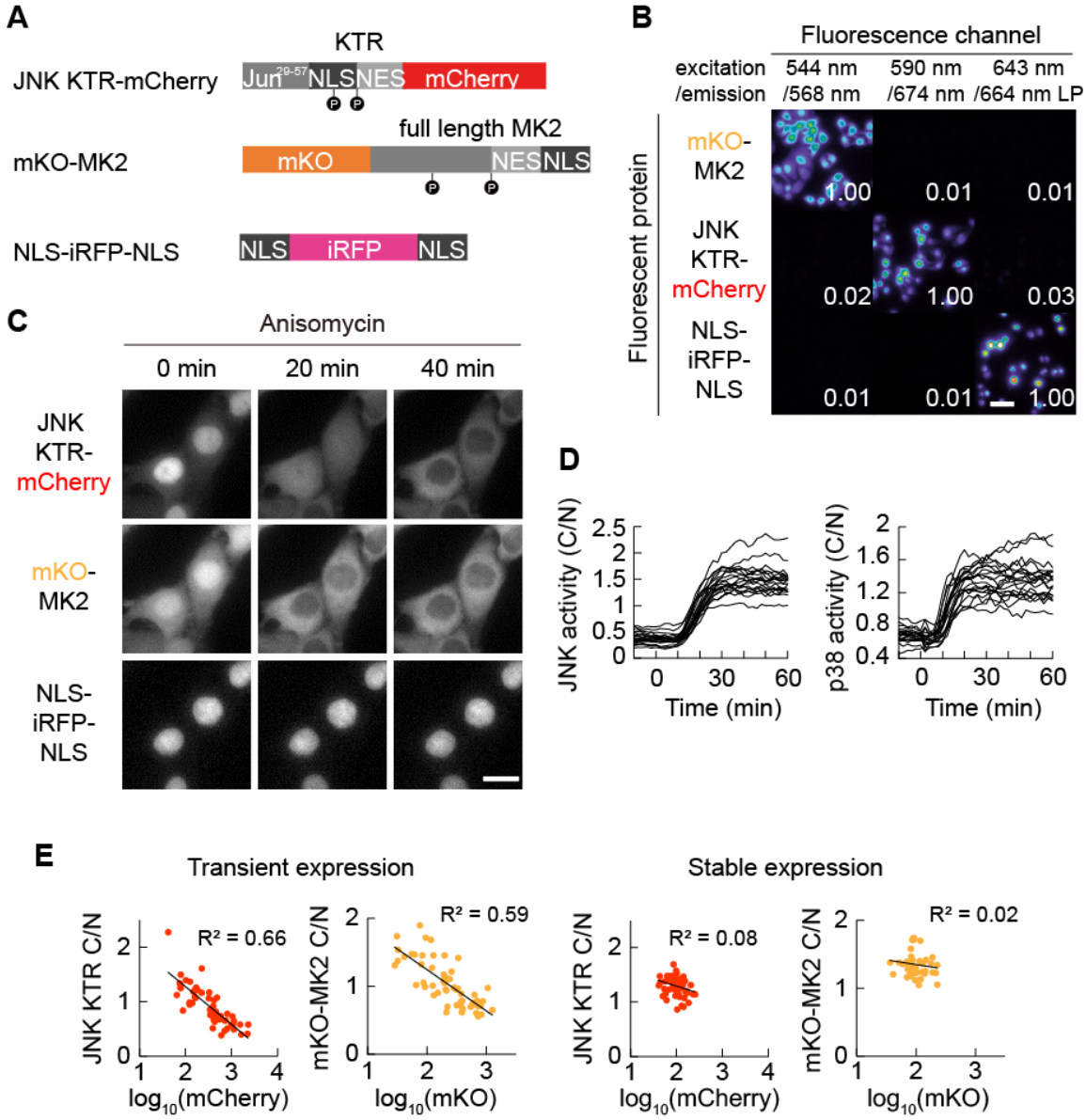

Figure 6. Establishment of a multiplexed imaging system for monitoring JNK and p38 kinase activities.
(A) Structure of the JNK reporter JNK KTR-mCherry, p38 reporter mKO-MK2, and nuclear marker NLS-iRFP-NLS. NLS, nuclear localization signal; NES, nuclear export signal.
(B) Bleed-through analysis of HeLa cells individually expressing JNK KTR-mCherry, mKO-MK2, or NLS-iRFP-NLS. Representative images are shown in a pseudo-color scale. The values indicate the fraction of fluorescence leakage. Scale bar: 60 μm.
(C) Clonal HeLa reporter cells were treated with 1 μg/ml anisomycin and imaged over time. Scale bar: 20 μm.
(D) JNK KTR-mCherry and mKO-MK2 C/N ratios were quantified for single cells from (C). n = 20 cells each.
(E) HeLa cells transiently or stably expressing JNK KTR-mCherry and mKO-MK2 were stimulated with 1 μg/ml anisomycin for 60 min. Correlations of the C/N ratios with the single cell expression levels are shown. Pearson correlation values from linear regression are indicated. n ≥ 40 cells for each condition.

To achieve stable expression of all three reporter proteins at equimolar concentrations, next I generated a polycistronic plasmid named pNJP (Nuclear, JNK, and p38 reporter). This vector encoded NLS-iRFP-NLS, JNK KTR-mCherry, and mKO-MK2, linked by self-

cleaving P2A peptide sequences in the piggyBac backbone (Figure 7A). HeLa cells stably expressing NJP showed localizations of JNK KTR-mCherry, mKO-MK2, and NLS-iRFP-NLS that were comparable to those of the individually expressed reporters (Figures 6C and 7B), indicating that the reporters were successfully separated from each other. This was further confirmed by western blot analysis against mCherry and mKO, showing bands corresponding to JNK KTR-mCherry (~33.6 kDa) and mKO-MK2 (~70.2 kDa) (Figure 7C).

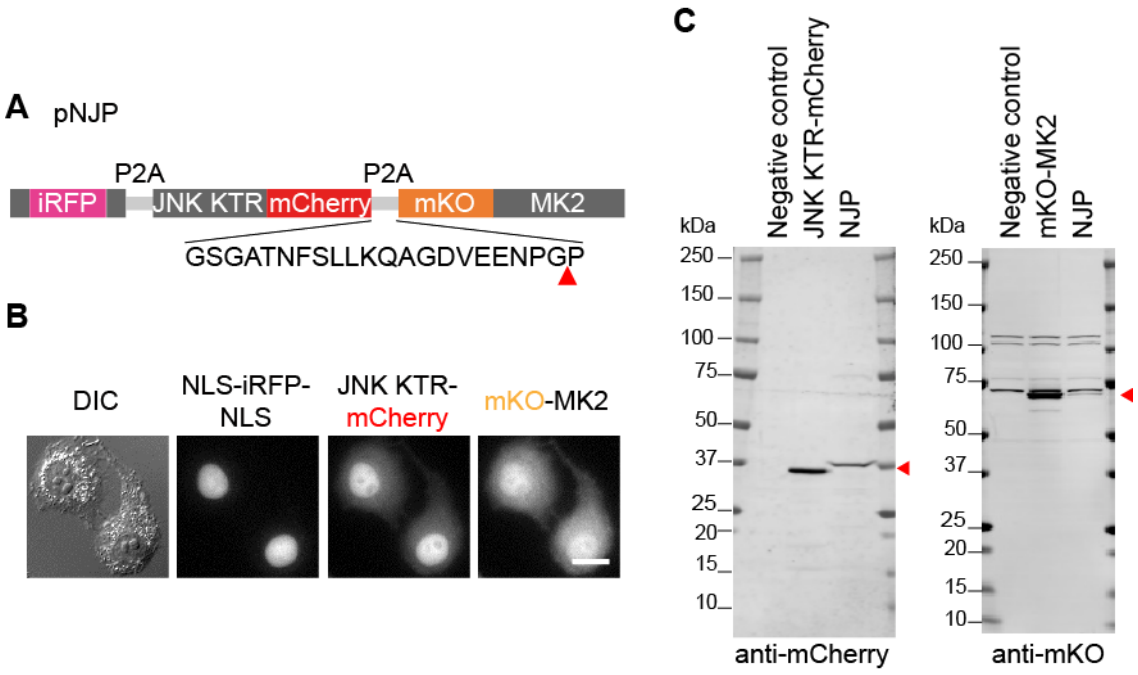

Figure 7. Development of a polycistronic reporter construct NJP.
(A) Structure of the polycistronic pNJP reporter, comprising NLS-iRFP-NLS, JNK KTR-mCherry, and mKO-MK2, connected by self-cleaving P2A sequences. The point of cleavage is indicated by a red arrowhead.
(B) Representative images of NLS-iRFP-NLS, JNK KTR-mCherry, and mKO-MK2 stably expressed from pNJP in HeLa cells. Scale bars: 20 μm.
(C) Western blot analysis of HeLa cells which stably expressed pNJP with anti-mCherry and anti-mKO. HeLa wildtype cells served as negative control and JNK KTR-mCherry (33.6 kDa) or mKO-MK2 (70.2 kDa) expressing cells as positive controls (red arrowhead).

3-2 Specificity and sensitivity of mKO-MK2 and JNK KTR-mCherry

Next, I evaluated the specificity of the reporters by small-molecule inhibitors and gene KO experiments. JNK inhibitor VIII, but not the p38 inhibitor SB203580 instantly reduced the anisomycin-stimulated increase in the C/N ratio of JNK KTR-mCherry (Figure 8A, top). Interestingly, p38 inhibition rather increased the C/N ratio of JNK KTR-mCherry, as discussed in detail in a later section (Figure 8A, top, orange line). As expected, the increase in

the C/N ratio of mKO-MK2 was repressed after addition of SB203580, while JNK inhibitor VIII had no effect (Fig. 8A, bottom). Moreover, *MAPK8* (*JNK1*) and *MAPK9* (*JNK2*) double KO completely suppressed the anisomycin-induced increase in the C/N ratio of JNK KTR-mCherry, while *MAPK14* (*p38α*) KO slightly enhanced the C/N ratio of JNK KTR-mCherry, comparable to the effect of p38 inhibition (Figure 8B, top). As anticipated, translocation of mKO-MK2 was largely prevented in *p38α* KO cells, but was unaffected by *JNK1/2* KO (Figure 8B, bottom). The KO of *JNK1/JNK2* and *p38α* was confirmed by western blot analysis (Figure 8C).

To further validate the dynamics of JNK KTR-mCherry and mKO-MK2, I compared the time courses of the C/N ratios to the endogenous phosphorylation of bulk JNK and p38 obtained by immunoblotting (Figure 8D). The kinetics of the change in the JNK KTR-mCherry and mKO-MK2 C/N ratios upon stimulation with anisomycin were comparable to those of JNK and p38 phosphorylation, respectively, with a time lag of 5 to 10 min (Figure 8E); the lag may have been attributable to the delayed substrate phosphorylation after kinase activation and/or nucleocytoplasmic shuttling.

Taken together, these data demonstrate that JNK KTR-mCherry and mKO-MK2 reliably monitor JNK and p38α activities, respectively.

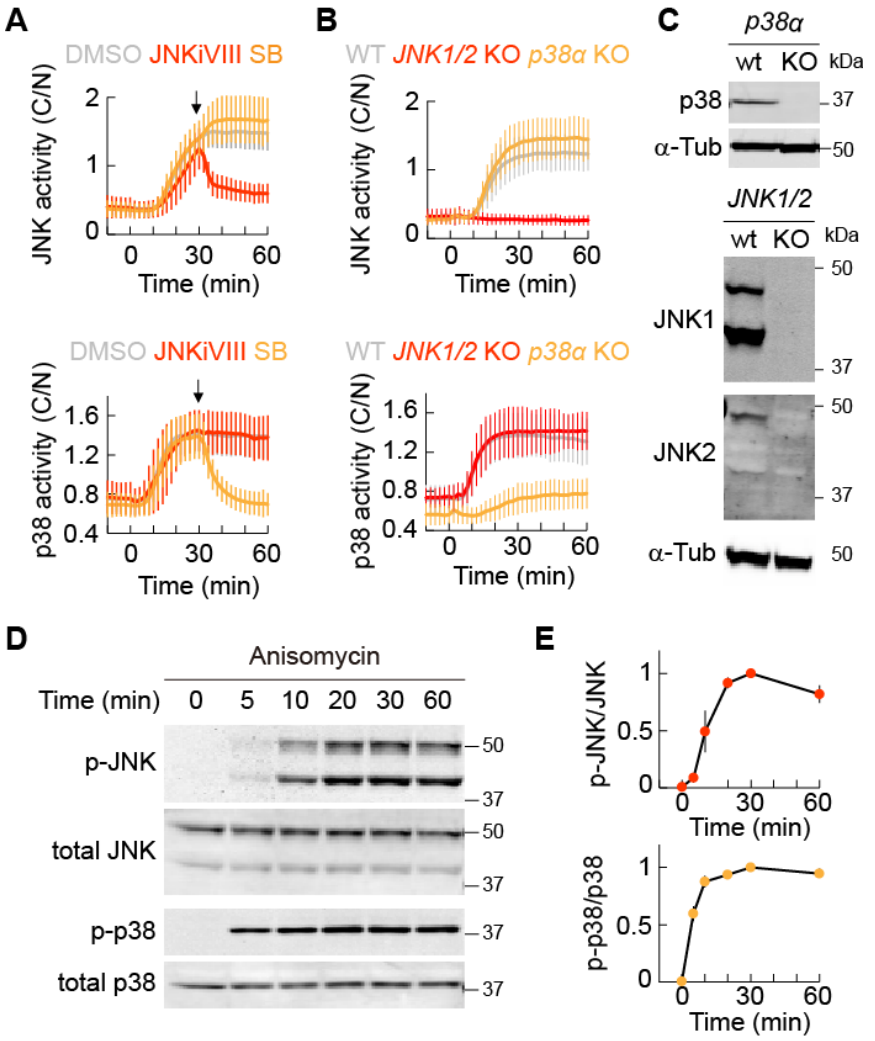

Figure 8. Specificity of JNK KTR-mCherry and mKO-MK2.
(A) Clonal HeLa reporter cells were stimulated with 1 µg/ml anisomycin and after 30 min treated with 10 µM JNK inhibitor VIII (JNKiVIII), 10 µM SB203580 (SB), or 0.1% DMSO (arrow). Mean JNK KTR-mCherry and mKO-MK2 C/N ratios with SD are shown. n = 40 cells each from two independent experiments.
(B) HeLa wildtype, *MAPK8/9* (*JNK1/2*) double KO, and *MAPK14* (*p38α*) KO cells expressing NJP were stimulated with 1 µg/ml anisomycin. Mean JNK KTR-mCherry and mKO-MK2 C/N ratios with SD are shown. n = 20 cells each from one representative experiment.
(C) Western blot analysis of *MAPK14* (*p38α*) KO and *MAPK8* (*JNK1*) *MAPK9* (*JNK2*) double KO with antibodies against total p38, JNK1, JNK2, and α-tubulin as a control.
(D) Western blot analysis of endogenous JNK and p38 phosphorylation in 1 µg/ml anisomycin treated HeLa cells. Representative blots out of three independent experiments are shown.
(E) Time courses of p-JNK/JNK and p-p38/p38 ratios upon 1 µg/ml anisomycin stimulation from Western blot analysis from (A). All time courses were normalized between 0 and 1 using minimum and maximum values and presented as the mean with SD. n = 3 independent experiments.

For assessment of the sensitivity and dynamic range of the reporters, I studied their dose-dependent response to anisomycin (Figure 9A). Both, mKO-MK2 and JNK KTR-mCherry, demonstrated a moderately switch-like response of the C/N ratios (Figure 9B). Under the same conditions, phosphorylation of p38 (Thr180 and Tyr182) and JNK (Thr183 and

Tyr185), which are the activation markers, also exhibited a similar dose-response to anisomycin (Figure 9C). Direct comparison of the C/N ratios and normalized levels of phosphorylated protein kinase demonstrated a strong linear correlation (Figure 9D). These data imply that the dynamic range of the translocation reporters covers the full range of JNK and p38 activity following anisomycin stress. In conclusion, the results showed that this system allows us to quantitatively monitor stress-induced p38 and JNK activity-dynamics with high specificity and sensitivity at the single cell level.

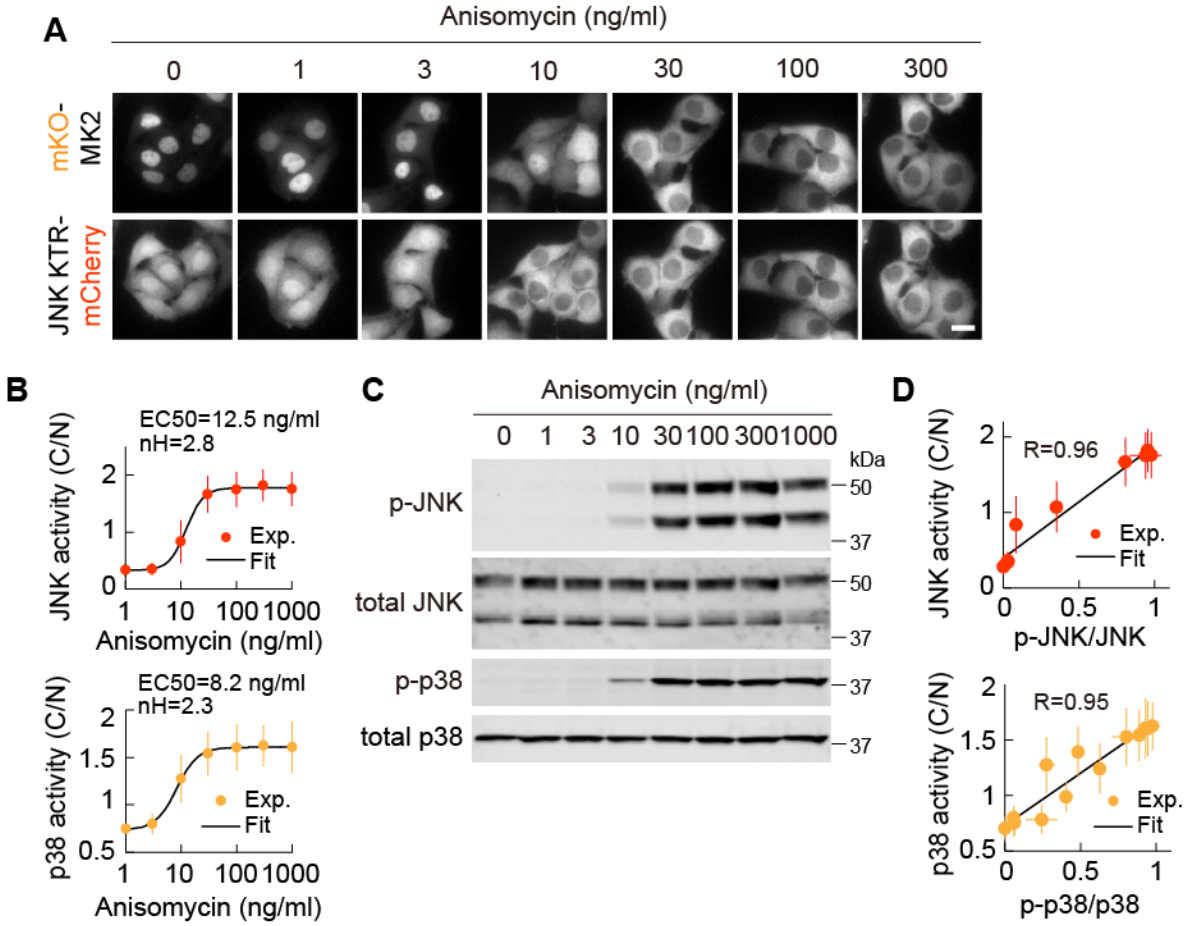

Figure 9. Sensitivity of JNK KTR-mCherry and mKO-MK2.
(A) Titration of HeLa reporter cells with anisomycin for 1 h. Representative images are given. Scale bar: 20 µm.
(B) Dose-response curves of the JNK KTR-mCherry and mKO-MK2 C/N ratios after 1 h anisomycin treatment. Experimental data are presented as the mean with SD and were fitted with the Hill function. Derived EC50 values and Hill coefficients (nH) are indicated. n ≥ 100 cells each, from at least three independent experiments.
(C) Western blot analysis of endogenous p38 and JNK phosphorylation in HeLa cells after 1 h anisomycin titration. Representative blots out of three independent experiments are shown.
(D) Correlation of JNK KTR-mCherry and mKO-MK2 C/N ratios with normalized p-JNK/JNK and p-p38/p38 ratios, respectively. Data were obtained after 1 h treatment with various doses of anisomycin and/or SB203580 and are presented as the mean with SD.Pearson correlation values from a linear regression are shown. n = 3 for western blot data and n ≥ 60 cells for imaging data.

3-3 Basal p38 and JNK activities during cell cycle progression

Since a role of JNK and p38 in cell cycle progression had been proposed in literature (MacCorkle and Tan, 2005), I investigated the JNK and p38 activities without addition of any external stress stimuli. The basal JNK and p38 activities in single cells were monitored over entire cell cycles for two days, aligned at mitotic exit and displayed till mitotic entry (Figure 10). Interestingly, JNK and p38 activities showed inverse patterns: JNK activity was low in the first half of the cell cycle and started to increase in the latter half of the cell cycle with an acute peak at the G2/M transition (Figure 10A and 10B). In contrast, p38 activity rose slightly in the first half of cell cycle and decreased again in the second half of the cell cycle (Figure 10A and 10B). Our data confirmed previous biochemical studies reporting that JNK activity is high in G2 phase and early mitosis (Gutierrez et al., 2010) and p38 signaling needs to be inactivated for the G2/M progression (Ambrosino and Nebreda, 2001; Bulavin et al., 2001; Thornton and Rincon, 2009).

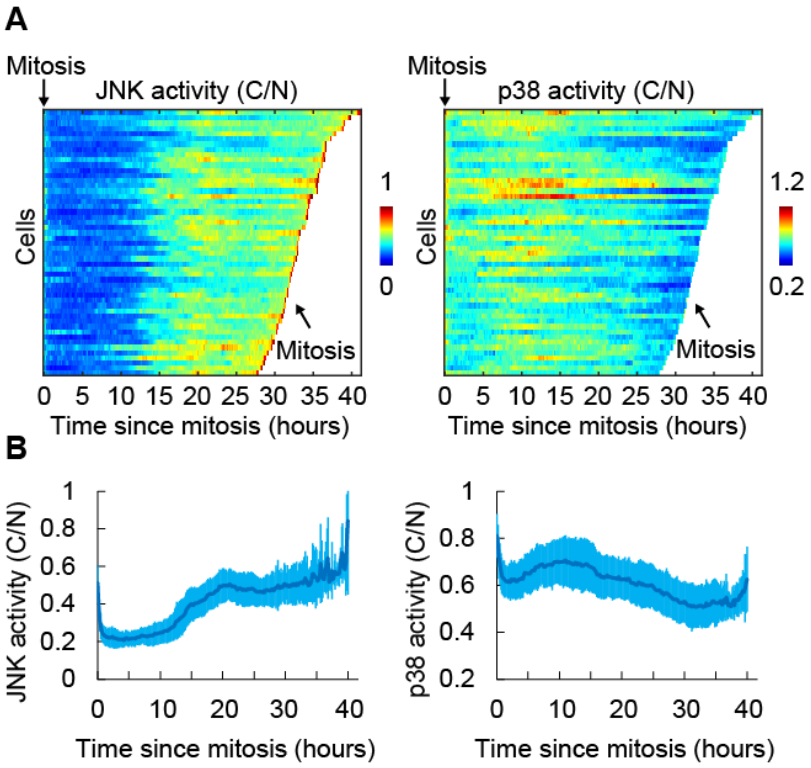

Figure 10. Basal JNK and p38 activities during cell cycle.
(A) Clonal HeLa reporter cells were imaged without stimulation. Single cell JNK KTR-mCherry and mKO-MK2 C/N ratios are displayed as heat maps from mitotic exit to mitotic entry. Each line represents the activity dynamics in a single cell, with red colors indicating high and blue colors indicating low kinase activities. n = 51 cells from one representative experiment.
(B) Mean JNK KTR-mCherry and mKO-MK2 C/N ratios with SD are shown for cells from (A). n = 51 cells.

3-4 Crosstalk between JNK and p38 signaling pathways

In the past decades, an increasing number of studies has provided compelling evidence of the interplay of p38 and JNK pathways at a population level. Pharmacological inhibition and KO of *p38α* caused JNK hyper-activation in cell lines and mouse models, indicating that p38 signaling suppresses JNK activity (Caballero-Franco et al., 2013; Cheung et al., 2003; Heinrichsdorff et al., 2008; Hui et al., 2007; Jones et al., 2018; Kim et al., 2008; Perdiguero et al., 2007; Pereira et al., 2013; Staples et al., 2010). Thus, the inhibition of JNK by p38 seems to be a fundamental mechanism in the control of SAPK signaling. Although this crosstalk has been well-documented in cell populations, it is basically unstudied how it regulates dynamical patterns and cell-to-cell variation of SAPK signaling at single-cell resolution.

The aforementioned imaging system for p38 and JNK activities provides a potent tool to investigate the crosstalk of p38 and JNK in individual cells. For this purpose, clonal HeLa reporter cells were pretreated with DMSO or p38 inhibitors and then stimulated with two pro-inflammatory cytokines, TNFα and interleukin-1β (IL-1β), or three stress inputs, anisomycin, sorbitol, and UV-C (Figures 11A and 11B). In control cells, I observed distinct kinetics of JNK and p38 activities for the different stimuli; TNFα and IL-1β stimulation resulted in transient JNK and p38 activation, while the other stress inputs induced JNK and p38 activities in a more sustained fashion within the time frame of observation (Figure 11B, grey lines). Interestingly, JNK activity showed substantial heterogeneity among single cells, whereas the p38 response appeared more uniform in each condition (Figure 11A). When p38 was inhibited by SB203580, JNK activity was significantly higher than in the DMSO-treated control cells in response to the inflammatory cytokines and stress conditions (Figure 11B, orange lines), and the cell-to-cell variability of JNK activity appeared to be lower (Figure 11A). Two different p38 inhibitors reproduced this observation for all the different stimuli; VX-745, an ATP-competitive p38 inhibitor, and BIRB 796, an allosteric p38 inhibitor, resulted in higher JNK activities than in the DMSO control (Figures 11B and 11C).

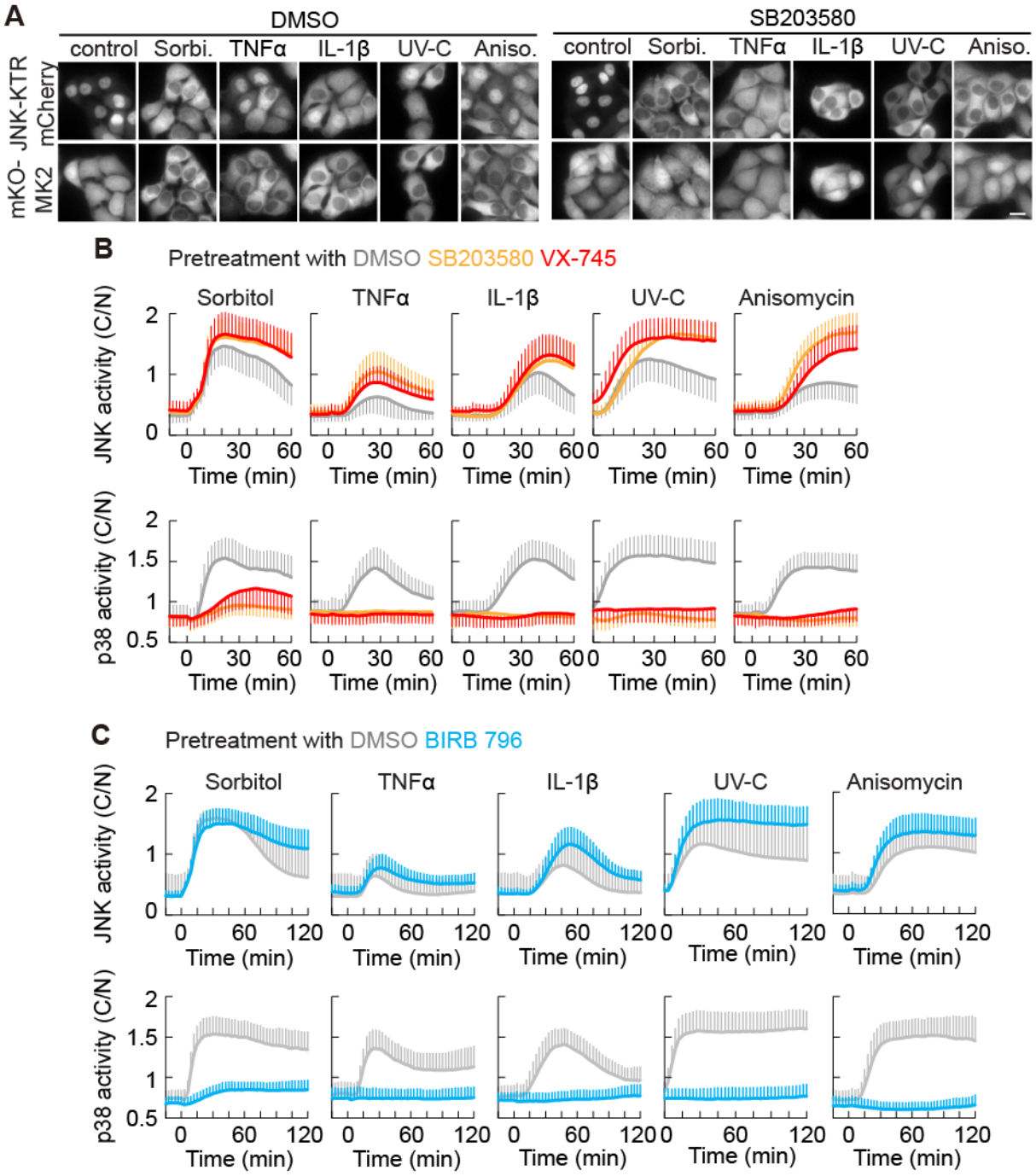

Figure 11. Cross-inhibition of JNK activity by p38 in various stress conditions.
(A) Clonal HeLa reporter cells were pretreated with 0.1% DMSO or 10 μM SB203580 and then stimulated with 200 mM sorbitol, 10 ng/ml TNFα, 10 ng/ml IL-1β, 100 J/m^2 UV-C, 10 ng/ml anisomycin or imaging medium as control. Representative images of JNK KTR-mCherry and mKO-MK2 after 30 min of TNFα treatment and 1 h of treatment with the other stimuli are shown. Scale bar: 20 μm.
(B-C) Clonal HeLa reporter cells were pretreated with 0.1% DMSO, 10 μM SB203580, 1 μM VX-745, or 0.5 μM BIRB 796 and then stimulated at elapsed time 0 min as described in (A). Mean JNK KTR-mCherry and mKO-MK2 C/N ratios with SD are shown. n ≥ 50 cells each from two independent experiments.

To confirm the cross-inhibition of JNK by p38 at the endogenous level, I analyzed the endogenous activation of JNK after stress exposure by western blotting. In line with the

imaging results, SB203580 pretreatment resulted in significantly higher levels of phospho-JNK (Thr183 and Tyr185) for all tested stimuli than DMSO pretreatment (Figure 12A, left). Interestingly, phosphorylation of p38 itself was unchanged by SB203580 pretreatment in the same samples (Figure 12 A, right), indicating that p38 does not induce negative feedback in the observed timescale, but rather specifically cross-inhibits JNK activity.

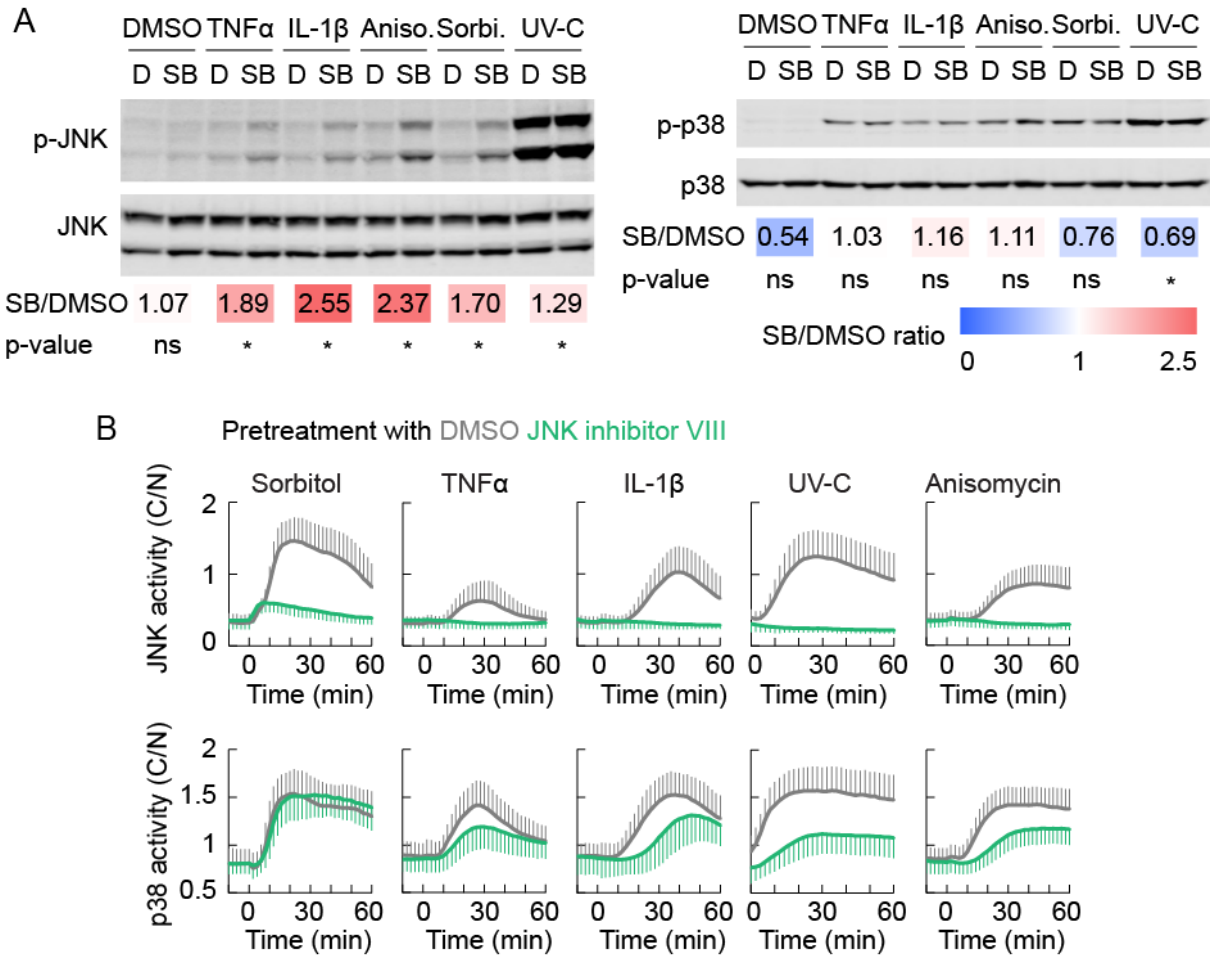

Figure 12. Crosstalk of JNK and p38 signaling pathways.
(A) Western blot analysis of the effect of SB203580 on JNK and p38 phosphorylation under various stresses. HeLa cells were pretreated with 0.1% DMSO (D) or 10 μM SB203580 (SB) and then stimulated with 10 ng/ml TNFα for 30 min and with the other stimulants 10 ng/ml IL-1β, 10 ng/ml anisomycin, 200 mM sorbitol, and 100 J/m^2 UV-C for 60 min. Representative blots out of three independent experiments are shown. The SB/DMSO ratio is the fold change of p-p38/p38 or p-JNK/JNK in the SB203580 over DMSO-treated samples. n=3 independent experiments. Significance was tested by a Student's *t*-test. ns = not significant, *p<0.05.
(B) Clonal HeLa reporter cells were pretreated with 0.1% DMSO or 10 μM JNK inhibitor VIII and then stimulated with 200 mM sorbitol, 10 ng/ml TNFα, 10 ng/ml IL-1β, 100 J/m^2 UV-C, or 10 ng/ml anisomycin. Mean JNK KTR-mCherry and mKO-MK2 C/N ratios with SD are shown. n = 50 each from two independent experiments.

I also tested the effect of JNK inhibition on p38 activity. Surprisingly, JNK inhibitor VIII partially reduced p38 activity in response to TNFα, IL-1β, anisomycin, and UV-C

(Figure 12B). This might indicate that JNK signaling positively regulates p38 activity, but the possibility of off-target effects of JNK inhibitor VIII could not be excluded. I therefore focused on the effect of p38 signaling on JNK activity in the present study.

To test how cross-inhibition of JNK by p38 desensitizes JNK activation upon anisomycin treatment, I examined the dose-dependency of JNK activities in control and SB203580-pretreated cells. SB203580 shifted the EC50 of the JNK response to lower concentration and converted the JNK activity response to a more switch-like output (Figure 13A). At the single cell level, JNK did not show an "all-or-none" response, but rather a graded response, as evidenced by the unimodal distribution of JNK activity (Figure 13B). This was especially evident for stimulation at around the EC50 concentration (7.5 ng/ml for SB203580 pretreatment), which yielded in only one peak of half maximal JNK activities (Figure 13B, right). Although bi-stability has been reported for individual anisomycin-stressed HeLa cells using a FRET biosensor (Fosbrink et al., 2010), meaning that cells either show a full or no response, our data suggest that the JNK activation was graded at the single cell level.

I also quantified the relationship of JNK and p38 activity over a range of SB203580 concentrations. SB203580 pretreatment dose-dependently reduced anisomycin-induced p38 activity and increased JNK activity (Figure 13C). Plotting JNK versus p38 activities for each inhibitor dose revealed a clear negative correlation of JNK and p38 activities, reinforcing that p38 signaling inhibits JNK activity (Figure 13D).

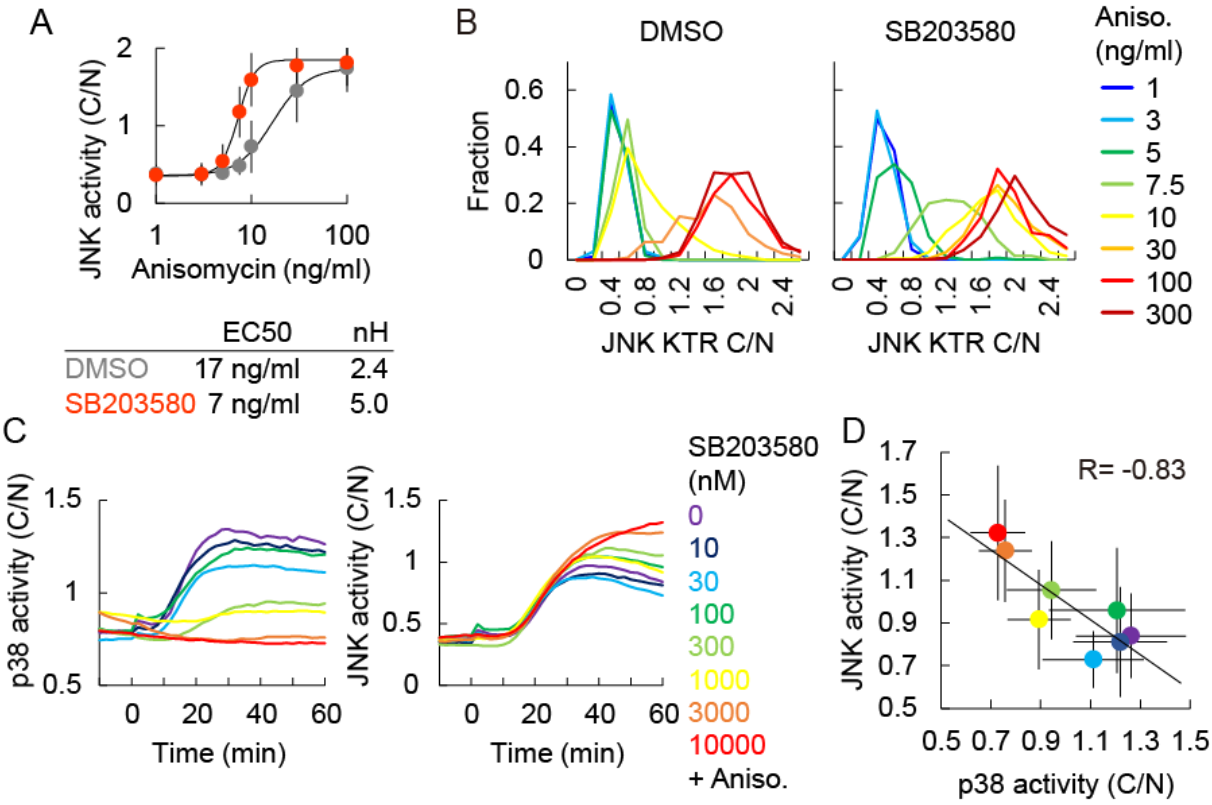

Figure 13. Cross-inhibition of JNK activity by p38.
(A) Clonal HeLa reporter cells were pretreated with 0.1% DMSO or 10 µM SB203580 and stimulated with various doses of anisomycin. Mean JNK KTR-mCherry C/N ratios with SD at 60 min of anisomycin treatment are shown. The dose responses were fitted with the Hill function (black lines). EC50 values and Hill coefficients (nH) are indicated. n ≥ 86 cells each from two independent experiments.
(B) Distributions of single cell JNK KTR-mCherry C/N ratios at 60 min of anisomycin treatment for 0.1% DMSO and 10 µM SB203580-pretreated cells from (A). n ≥ 86 cells each from two independent experiments.
(C) Clonal HeLa reporter cells stably were pretreated with the indicated doses of SB203580 and then stimulated with 10 ng/ml anisomycin. Mean JNK KTR-mCherry and mKO-MK2 C/N ratios are shown. n = 20 cells each.
(D) Correlation of JNK KTR-mCherry and mKO-MK2 C/N ratios (1 h after anisomycin stimulation) for conditions from (C). The Pearson correlation coefficient R from a linear regression model is indicated. Data are presented as the mean with SD. n = 20 cells each.

3-5 Transcriptional and post-translational cross-inhibition of JNK by p38

The next aim was to investigate the molecular mechanisms mediating the cross-inhibition of JNK by p38. As reviewed in the introduction, two possible mechanisms had been proposed: (1) p38 directly or indirectly regulates a MAPKK/MAPKKK upstream of JNK by post-translational modification, (2) p38 signaling induces transcription of *DUSP1*, which inactivates JNK. According to the current state of knowledge, the mode of cross-inhibition depends on the context, such as cell type and stimulus (Arthur and Ley, 2013; Wagner and Nebreda, 2009).

To determine the contribution of post-translational mechanisms, first I analyzed how fast p38 inhibition could induce JNK hyper-activation. We would expect that the inhibition through post-translational processes would lead to increased JNK activity on a faster time scale than the inhibition through transcriptional regulation. Indeed, treatment with SB203580 after stress exposure instantaneously led to higher JNK activity than the DMSO control in all tested conditions (Figure 14A), suggesting that fast post-translational mechanisms contributed to the early cross-inhibition of JNK for all tested stimuli.

To further differentiate the post-translational and transcriptional modes of cross-inhibition, I compared the effect of actinomycin D, which only inhibits transcriptional inhibition of JNK, to the effect of p38 inhibition by SB203580, which inhibits both modes of cross-inhibition (Figure 14B). SB203580 led to higher stimulant-induced JNK activities than actinomycin D in all conditions, indicating that post-translational processes were generally involved in suppression of JNK (Figure 14C, top panels). Actinomycin D considerably enhanced the JNK activation in response to IL-1β, UV-C, and anisomycin, but not to TNFα and sorbitol (Figure 14C, top panels). These results suggest that additional transcriptional mechanisms mediate suppression of JNK following IL-1β, UV-C, and anisomycin stress. With regard to p38 activities, actinomycin D prolonged the transient p38 activation by the cytokines, IL-1β and TNFα, but had no effect on the more sustained p38 activities induced by the other stimulants (Figure 14C, bottom panels), indicating that phosphatases induced by these stress stimuli did not inhibit p38, but rather specifically inactivated JNK.

The differences in the sensitivity to actinomycin D and SB203580 allowed to quantify how much transcriptional and post-translational mechanisms contribute to the cross-inhibition of JNK by p38 (Figure 14D). The difference of JNK activity between actinomycin D and DMSO control indicated the effect of transcriptional cross-inhibition, while the difference of JNK activity between SB203580 and actinomycin D pretreatment indicated the effect of a post-translational mechanism, as described in more detail in the materials and methods section. Interestingly, in the sorbitol (osmotic shock) and TNFα conditions, primarily, post-translational mechanisms drive cross-inhibition of JNK, whereas for IL-1β, UV-C, and anisomycin stress, both modes cooperate (Figure 14D).

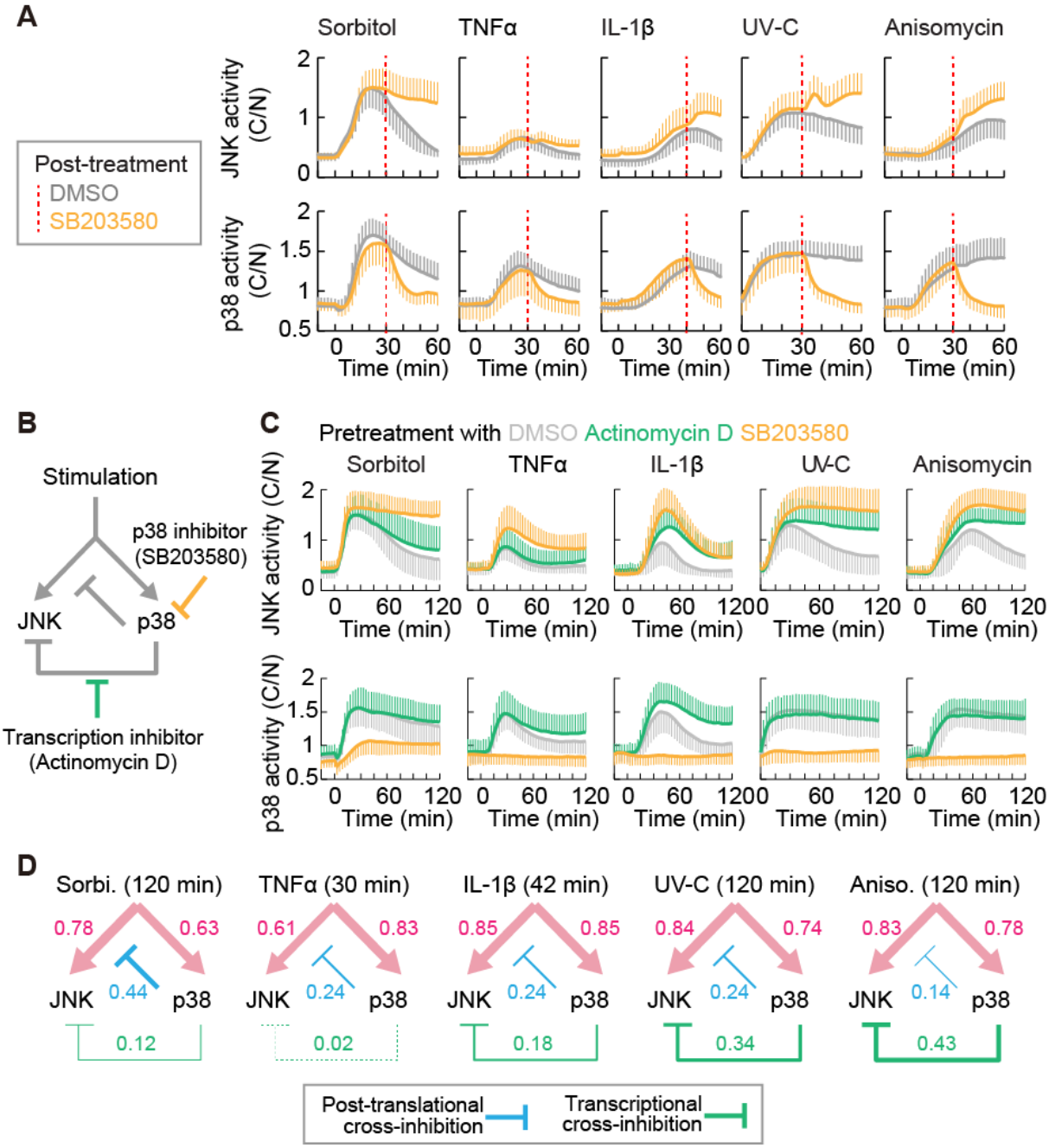

Figure 14. Post-translational and transcriptional cross-inhibition of JNK activity by p38.
(A) Clonal HeLa reporter cells were stimulated with 200 mM sorbitol, 10 ng/ml TNFα, 10 ng/ml IL-1β, 100 J/m^2 UV-C, or 10 ng/ml anisomycin and treated with 0.1% DMSO or 10 μM SB203580 at indicated time points (dashed line). Mean C/N ratios with SD are shown. n ≥ 20 cells for each condition.
(B) Scheme of cross-inhibition mechanisms of JNK by p38.
(C) Clonal HeLa reporter cells were pretreated with 0.1% DMSO, 1 μg/ml actinomycin D, or 10 μM SB203580, then treated with stimulants as described in (A). Mean C/N ratios with SD are shown. n = 70 cells each from at least two independent experiments.
(D) Strength of JNK and p38 activation and post-translational and transcriptional cross-inhibition for conditions from (C) at indicated time points. Edge thickness is proportional to the strength of pathway activities.

3-6 Transcriptional cross-inhibition of JNK by p38

Prior work had shown that p38 promotes *DUSP1* gene expression via activation of MSK1/2 and the transcription factor CREB; DUSP1 in turn inactivates JNK (Ananieva et al., 2008; Ferreiro et al., 2010; Kim et al., 2008; Staples et al., 2010).

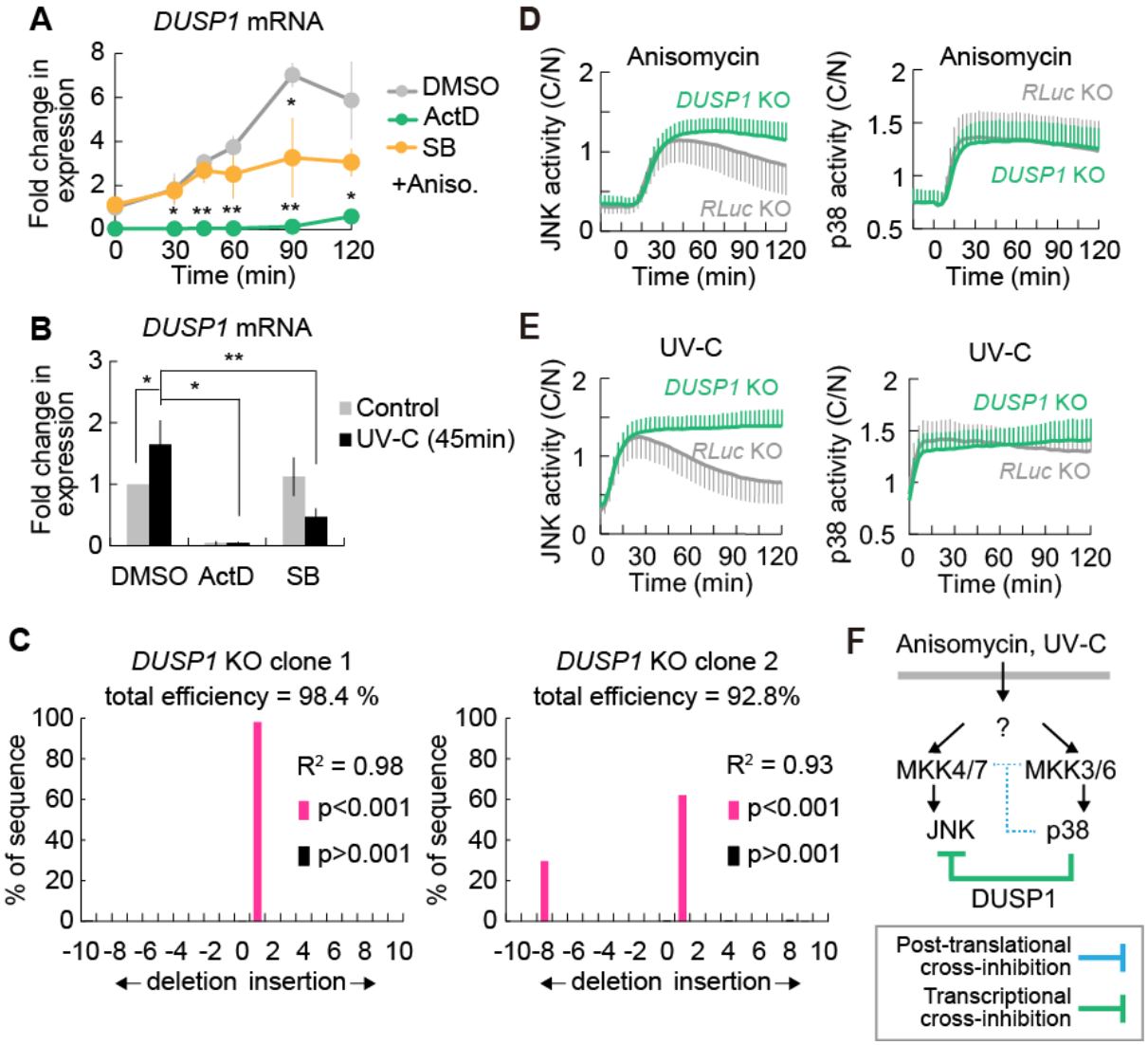

Figure 15. Transcriptional cross-inhibition of JNK by p38-induced *DUSP1* expression.
(A-B) Fold changes in *DUSP1* mRNA levels in 0.1% DMSO, 1 µg/ml actinomycin D, or 10 µM SB203580 pretreated HeLa cells after stimulation with 10 ng/ml anisomycin (A) or 100 J/m^2 UV-C (B). Data are shown as mean with SD. n = 3 independent experiments.
(C) Validation of *DUSP1* KO in clonal cell lines by sequencing and indel analysis of the *DUSP1* target locus.
(D-E) Time courses of JNK KTR-mCherry and mKO-MK2 C/N ratios in *DUSP1* KO and *RLuc* KO HeLa NJP cells after 10 ng/ml anisomycin (D) or 100 J/m^2 UV-C (E) stimulation. C/N ratios are shown as mean with SD. n = 50 cells for each condition from two independent experiments.
(F) Model of transcriptional cross-inhibition of JNK by p38-induced *DUSP1* gene expression.

Thus, I examined the role of DUSP1 in cross-inhibition of JNK by p38 in anisomycin and UV-C stress conditions, which exhibited the strongest transcriptional mode of cross-inhibition. Indeed, anisomycin and UV-C stress induced *DUSP1* mRNA in a manner dependent on p38 (Figures 15A and 15B). To further study the effect of DUSP1, we established CRISPR/Cas9 mediated *DUSP1* KO cells. Frameshift insertions/deletions at the *DUSP1* target locus gene were confirmed by sequencing of two different clonal cell lines (Figure 15C). *DUSP1* KO cells showed increased and more sustained JNK activities than *RLuc* control KO cells upon anisomycin and UV-C stimulation, while no clear effect on p38 activities was observed (Figure 15D and 15E). These data strongly suggest that p38-induced DUSP1 is involved in suppression of JNK in response to anisomycin and UV-C (Figure 15F).

3-7 Post-translational cross-inhibition of JNK by p38

With regard to a post-translational mechanism of cross-inhibition, it had been reported that TAK1 and TAB1 were components of negative feedback regulation of MAPKs by p38 (Cheung et al., 2003). As outlined in the introduction, TAK1 is a MAPKKK upstream of the JNK and p38 pathways (Ninomiya-Tsuji et al., 1999) and its adapter protein TAB1 binds to and thus activates TAK1 kinase (Mendoza et al., 2008; Shibuya et al., 1996). It has been proposed that p38-mediated phosphorylation of TAB1 reduces TAK1 and downstream kinase activities in response to proinflammatory cytokines and LPS (Cheung et al., 2003) (Figure 16A).

To examine whether the TAK1/TAB1 complex was involved in the regulation of JNK by p38 following cytokine stimulation, I first assessed whether JNK and p38 activities were dependent on TAB1 and TAK1 by using CRISPR/Cas9-mediated KO cells. Depletion of TAB1 and TAK1 protein was confirmed in KO cell lines by western blotting (Figure 16B and 16C). On the one hand, *TAB1* and *MAP3K7* (*TAK1*) KO completely prevented TNFα- and IL-1β-induced JNK activities (Figure 16D). On the other hand, TNFα-stimulated p38 activation was only dependent on TAK1, but surprisingly not TAB1 (Figure 16E). IL-1β-induced p38 activation was partially suppressed in *TAK1* KO and *TAB1* KO cells (Figure 16E). Since TAB1 phosphorylation by p38 likely has a pivotal role in JNK activity inhibition (Cheung et al., 2003), I constructed non-phosphorylatable alanine mutants of the p38 phosphorylation sites in TAB1, namely Ser423 and Thr431, and predicted that this TAB1 SATA mutant could rescue and even increase JNK activity in *TAB1* KO cells. While TAB1 wildtype rescued JNK

activation in response to TNFα and IL-1β, expression of TAB1 SATA resulted in even higher JNK activities (Figure 16D). In contrast, TAB1 SATA mutation had no effect on p38 activation (Figure 16E), suggesting that phosphorylation of TAB1 on Ser423 and Thr431 reduces TAK1 activity towards JNK, but probably not p38 in living cells. In summary, my imaging system confirms that phosphorylation of TAB1 by p38 mediates posttranslational cross-inhibition of JNK in response to pro-inflammatory cytokines.

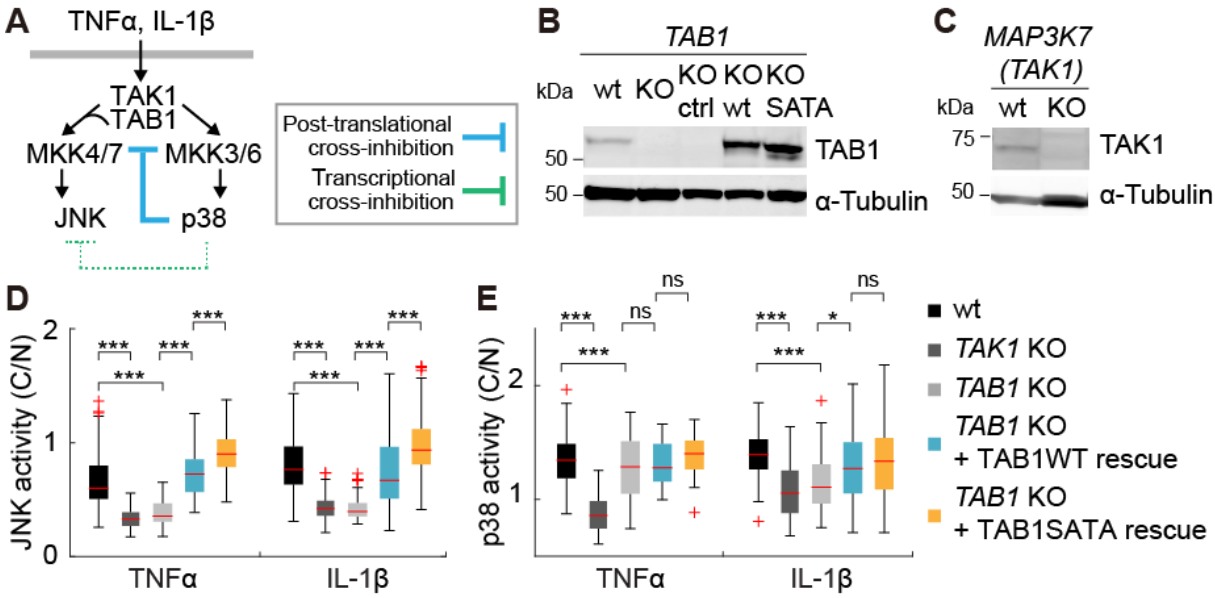

Figure 16. Post-translational cross-inhibition of JNK by p38-mediated TAB1 phosphorylation.
(A) Model of post-translational cross-inhibition of JNK by p38-mediated TAB1 phosphorylation.
(B) Western blot analysis of the TAB1 in HeLa wildtype (wt) cells, *TAB1* KO cells, *TAB1* KO cells expressing an empty control construct, *TAB1* KO cells complemented with TAB1-wt or TAB1 S423A T431A (SATA).
(C) Western blot analysis of TAK1 in HeLa wt and *MAP3K7* (*TAK1*) KO cells.
(D-E) JNK KTR C/N and mKO-MK2 C/N ratios in NJP expressing HeLa wt, *TAK1* KO, *TAB1* KO cells, and *TAB1* KO cells complemented with TAB1-wt or TAB1-SATA after stimulation with 10 ng/ml TNFα for 30 min or 10 ng/ml IL-1β for 50 min. The central line, top and bottom edges indicate the median, 25th, and 75th percentiles, respectively, with the whiskers denoting 1.5 times the interquartile range. Red crosses are outliers. n ≥ 37 cells for each condition from at least two independent experiments. Significance was tested against the wt control by a Student's *t*-test. ns, not significant; *p<0.05, **p<0.01, ***p<0.001.

3-8 Cross-inhibition by p38 generates cell-to-cell heterogeneity in JNK activity

Since the consequence of SAPK crosstalk on the single cell kinase activities has remained virtually unstudied in the literature, I was keen to examine the effect of p38-mediated cross-inhibition on the cell-to-cell heterogeneity in JNK activity. As mentioned before, I found that

stress- and cytokine-dependent JNK activities varied greatly among single cells, whereas p38 activities appeared more uniform in the same cells (Figure 11A). To quantitate cell-to-cell heterogeneity, I henceforward apply the coefficient of variation (CV) of C/N ratios, which is simply calculated by the ratio of SD and mean. For example, anisomycin- induced JNK activities had a broad distribution with a CV of ~ 0.39, compared to a relatively small CV of ~ 0.21 for p38 activities (Figure 17A). Strikingly, when cells were pretreated with p38 inhibitor, the elevated JNK activities exhibited reduced cell-to-cell variation with a CV of ~ 0.18 (Figure 17A). The time course of the CV reflected this finding; upon anisomycin stimulation the CV of JNK activity increased gradually and modestly, while in presence of SB203580, the CV of JNK activity declined remarkably over time (Figure 17B). Noteworthy, the CV of JNK activity plateaued to the minimum around 30 min after anisomycin stimulation in SB203580-pretreated cells, although the JNK activity had not reached its maximum at that time yet (Figures 11B and 14C). This comparison indicates that the reduced CV was not the result of saturation of JNK activity or limiting dynamic range. Consistently, anisomycin stress in *MAPK14* (*p38α)* KO cells led to lower cell-to-cell variability of JNK activity than in control cells (Figures 17C and 17D). This SB203580-induced decline of the CV of JNK activity was also observed for other stimuli. SB203580 led to smaller CVs of JNK activity in response to TNFα, IL-1β, sorbitol, and UV-C, in comparison to the control (Figure 17E). We thus hypothesize, that p38-mediated cross-inhibition of JNK generates cellular heterogeneity in JNK activity.

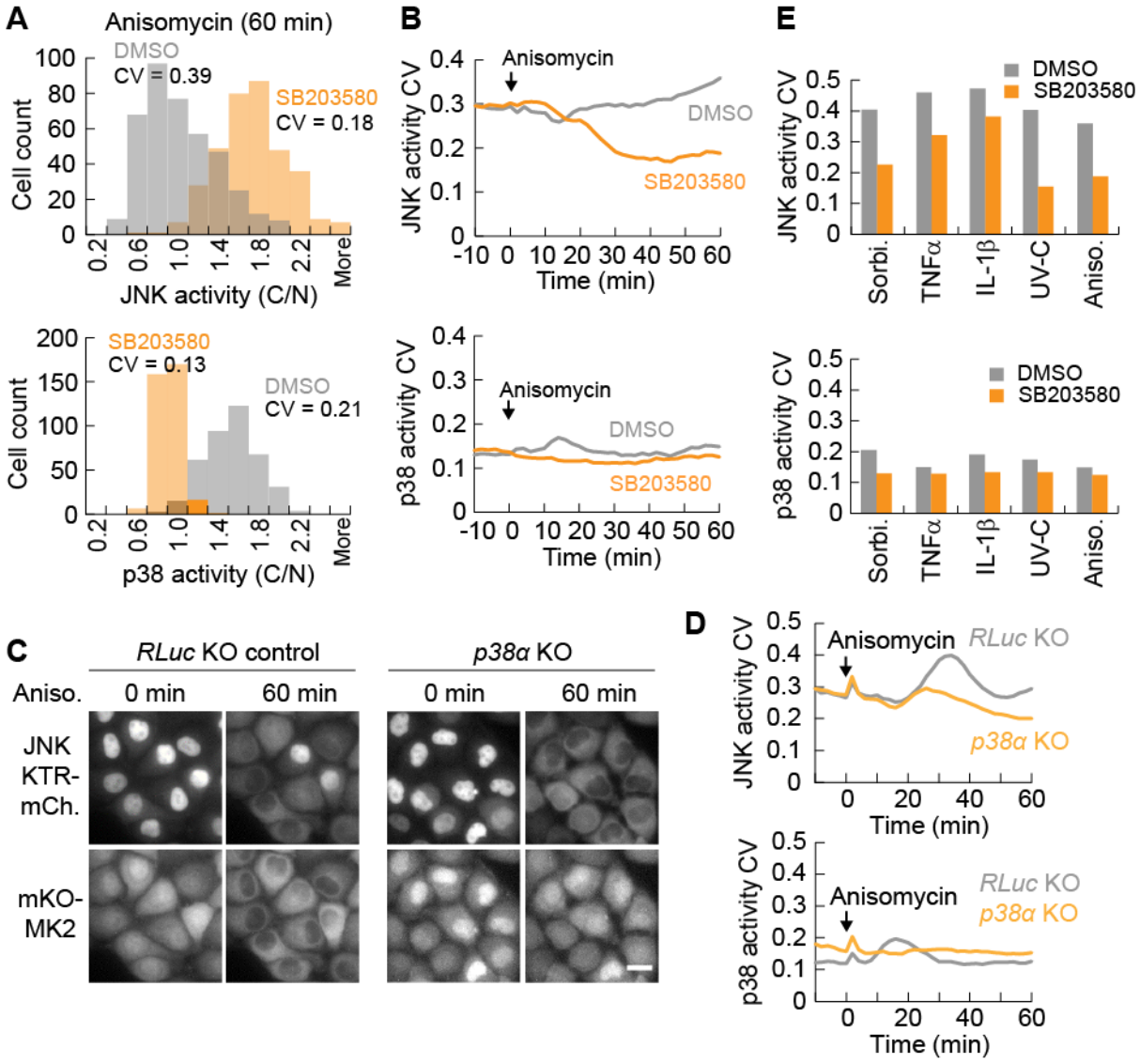

Figure 17. Cross-inhibition of JNK by p38 generates cell-to-cell heterogeneity in JNK activity.
(A) Histograms of the single cell JNK KTR-mCherry and mKO-MK2 C/N ratios in 0.1% DMSO or 10 μM SB203580-pretreated clonal HeLa reporter cells after 60 min treatment with 10 ng/ml anisomycin. The coefficient of variation (CV) is denoted. n ≥ 350 cells per condition from four independent experiments.
(B) The time course of the CV of the JNK KTR-mCherry and mKO-MK2 C/N ratios in 0.1% DMSO or 10 μM SB203580-pretreated clonal HeLa reporter cells upon 10 ng/ml anisomycin stimulation. n = 50 cells each from two independent experiments.
(C) Representative images of JNK KTR-mCherry and mKO-MK2 in NJP expressing HeLa *p38α* KO and *RLuc* KO cells upon stimulation with 10 ng/ml anisomycin. Scale bar: 20 μm.
(D) The time courses of CV of JNK KTR-mCherry and mKO-MK2 C/N ratios for cells from (C). n = 110 cells for *p38α* KO and 120 cells for *RLuc* KO from two independent experiments.
(E) The CV of the JNK KTR-mCherry and mKO-MK2 C/N ratios at 30 min treatment with 10 ng/ml TNFα and 60 min treatment with the other stimuli 200 mM sorbitol, 10 ng/ml IL-1β, 100 J/m^2 UV-C, and 10 ng/ml anisomycin is shown for 0.1% DMSO or 10 μM SB203580-pretreated clonal HeLa reporter cells. n = 50 cells per condition from two independent experiments.

Interestingly, the CV of p38 activity was constant upon anisomycin treatment (Figure 17B and 17D). Similar results were obtained with two different p38 reporters, p38 KTR and the FRET biosensor perky p38 NES (Figures 18A - 18F).

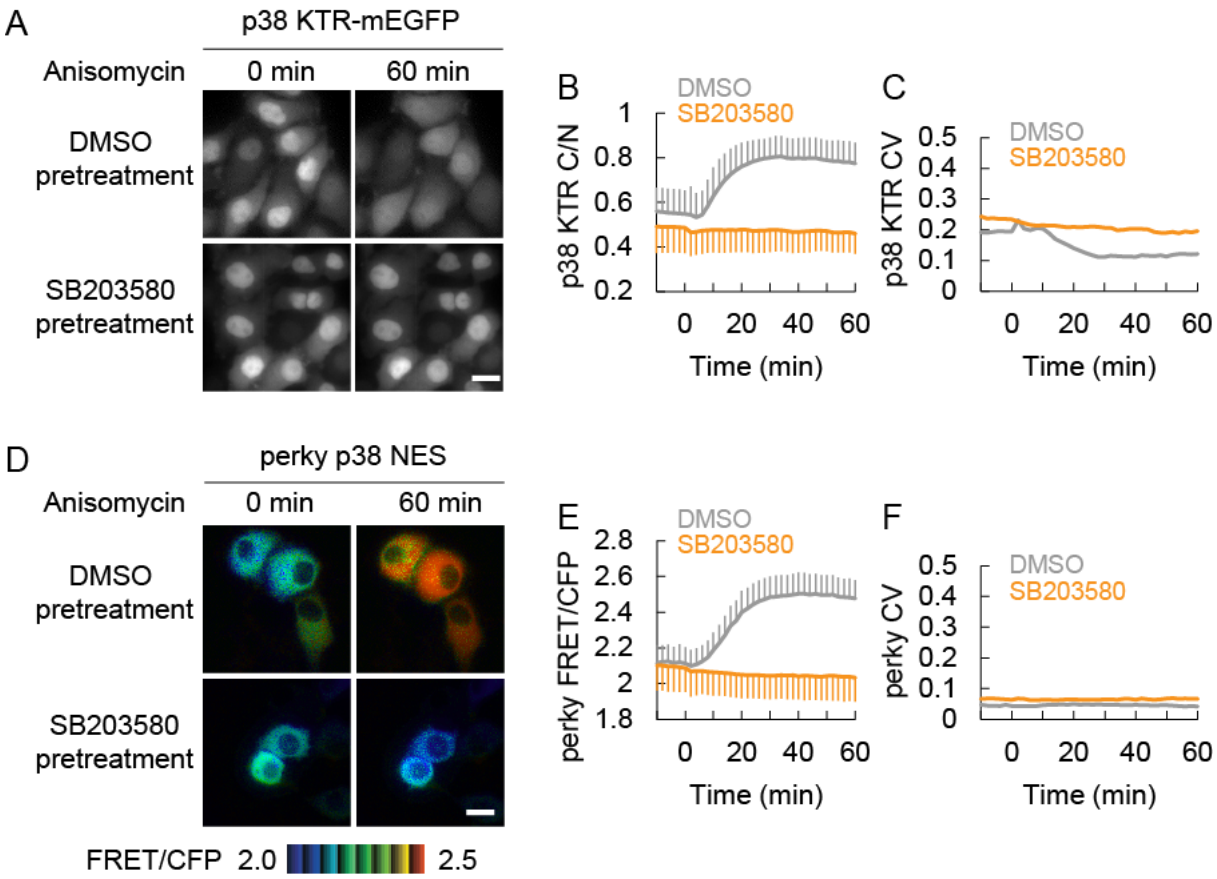

Figure 18. Cell-to-cell variability in p38 signaling.
(A-C) HeLa cells expressing p38 KTR-mEGFP were pretreated with 0.1% DMSO or 10 μM SB203580 and stimulated with 10 ng/ml anisomycin. Representative images of p38 KTR-mEGFP (A), the time courses of the mean p38 KTR-mEGFP C/N ratios with SD (B), and the CVs are shown (C). Scale bar: 20 μm. n = 75 cells for each condition from two independent experiments.
(D-F) HeLa cells transiently expressing perky p38 NES were pretreated with 0.1% DMSO or 10 μM SB203580 and stimulated with 10 ng/ml anisomycin. Representative ratio images in the IMD mode (D), the time courses of the mean FRET/CFP ratios with SD (E), and the CVs are shown (F). Scale bar: 20 μm. n = 50 cells for each condition from two independent experiments.

To test the generality of the observation, I examined the effect of SB203580 on JNK activity in various cell lines: A549, a lung cancer cell line; MCF10A, a normal-like human mammary epithelial cell line; and NIH3T3, a mouse embryonic fibroblast cell line. First of all, p38 inhibition potentiated and sustained UV-C-induced JNK activities in all cell lines. Second, the CV of JNK activity increased after UV-C stress exposure in all cell lines. And third, SB203580 remarkably reduced the CV of JNK activity in all tested cell lines (Figures

19A - 19F). Taken together, cross-inhibition of JNK by p38 produces cell-to-cell variability of JNK activity in a wide range of cell lines.

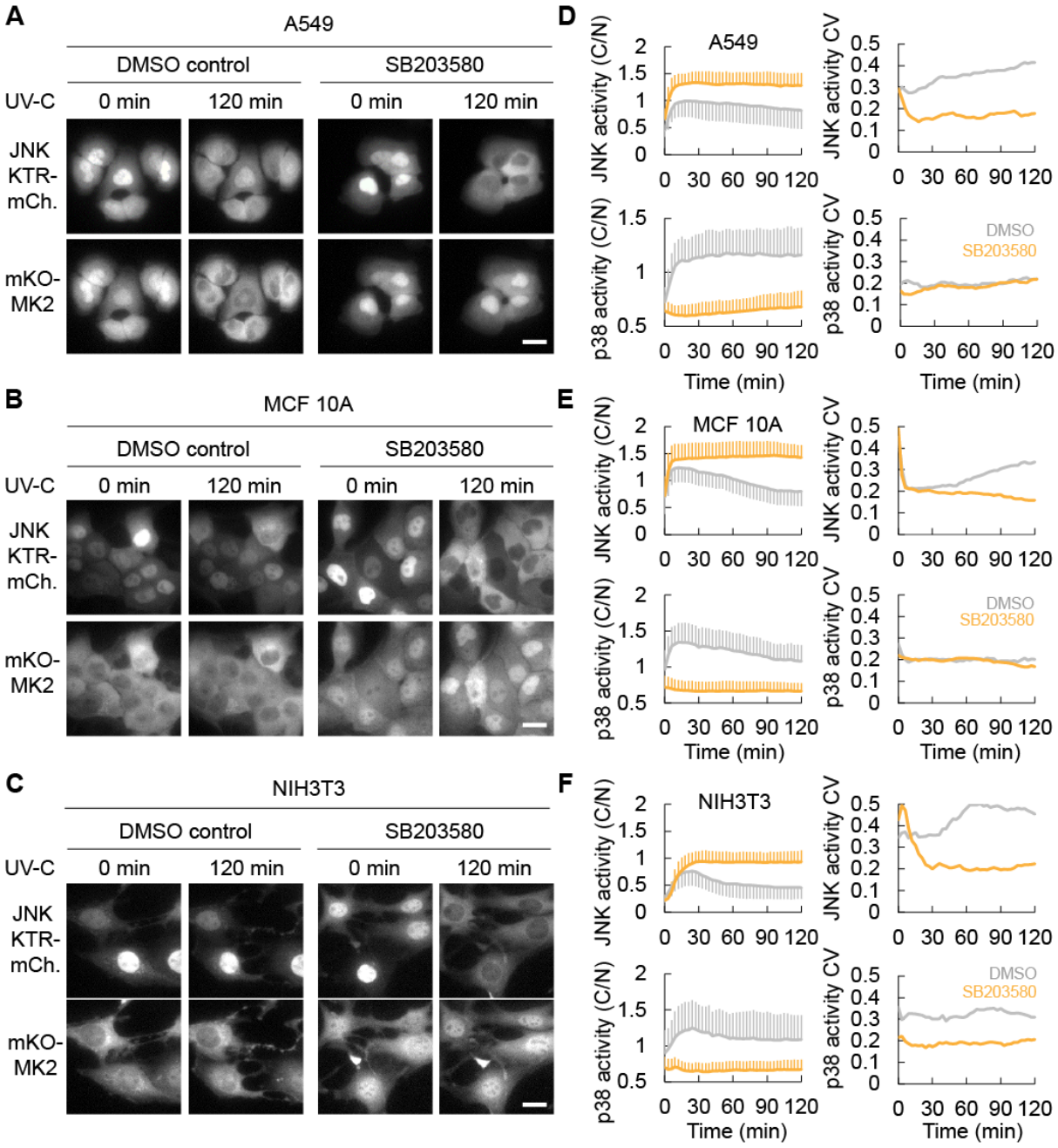

Figure 19. Cross-inhibition of JNK by p38 generates variability in JNK activity in various cell lines.
(A-C) Representative images of JNK KTR-mCherry and mKO-MK2 in NJP expressing A549 (A), MCF10A (B), and NIH3T3 cells (C) which were pretreated with 0.1% DMSO or 10 μM SB203580 and irradiated with 100 J/m^2 UV-C. Scale bar: 20 μm.
(D-F) Mean C/N ratios with SD and the time courses of the CV of JNK KTR-mCherry and mKO-MK2 C/N ratios are shown for cells from (A-C). n ≥ 24 cells from at least two independent experiments.

Furthermore, the CV of JNK activity substantially decreased over time in UV-C and anisomycin-stressed *DUSP1* KO cells, compared to the control cells (Figures 20A - 20D). The CV of p38 activity was not affected by the perturbation of *DUSP1* KO (Figures 20B and 20D). These findings point out that DUSP1 is involved in generation of variable JNK activities, and furthermore hint at the idea that noise in the p38-mediated *DUSP1* gene induction might be a potential source for the heterogeneity in JNK activities.

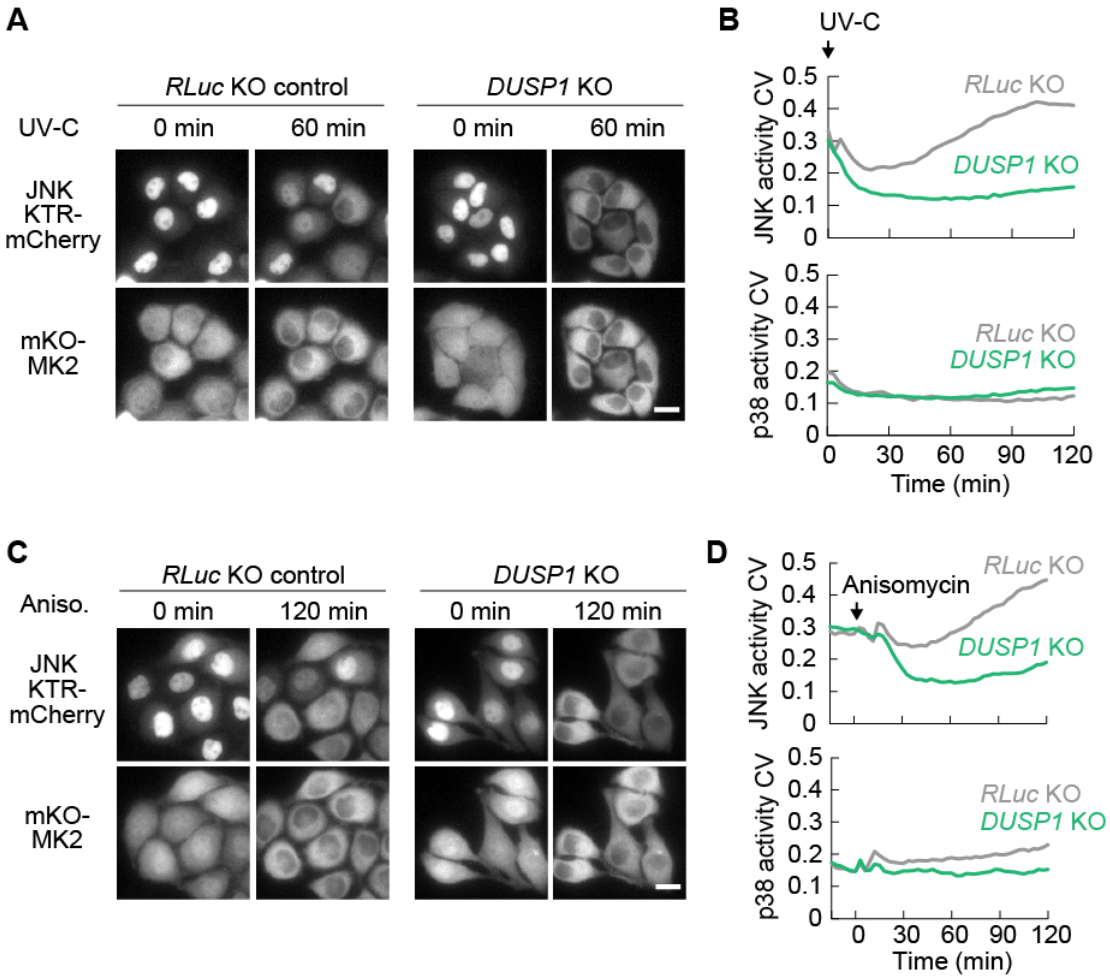

Figure 20. DUSP1 generates heterogeneity in JNK activity in response to anisomycin and UV-C.
(A) Representative images of JNK KTR-mCherry and mKO-MK2 in NJP expressing HeLa *DUSP1* KO and *RLuc* KO control cells upon irradiation with 100 J/m^2 UV-C. Scale bar: 20 μm.
(B) The time course of the CV of JNK KTR-mCherry and mKO-MK2 C/N ratios is depicted for NJP expressing *DUSP1* KO and *RLuc* KO control cells upon 100 J/m^2 UV-C stimulation. n = 50 cells per condition from two independent experiments.
(C) Representative images of JNK KTR-mCherry and mKO-MK2 in NJP expressing HeLa *DUSP1* KO and *RLuc* KO control cells upon stimulation with 10 ng/ml anisomycin. Scale bar: 20 μm.
(D) The time course of the CV of JNK KTR-mCherry and mKO-MK2 C/N ratios is shown for *DUSP1* KO and *RLuc* KO control cells upon 10 ng/ml anisomycin stimulation. n = 50 cells per condition from two independent experiments.

3-9 JNK activity correlates with fractional killing upon UV-C stress

The discovery of cross-inhibition-induced JNK activity heterogeneity leads to the question, whether this cell-to-cell variability in JNK activity impacts cellular phenotypes. To address this question, I chose UV-C-induced cell death as output, since it has been reported that JNK activity is necessary for UV-C-induced activation of the apoptosis pathway (Chen et al., 1996; Tournier et al., 2000).

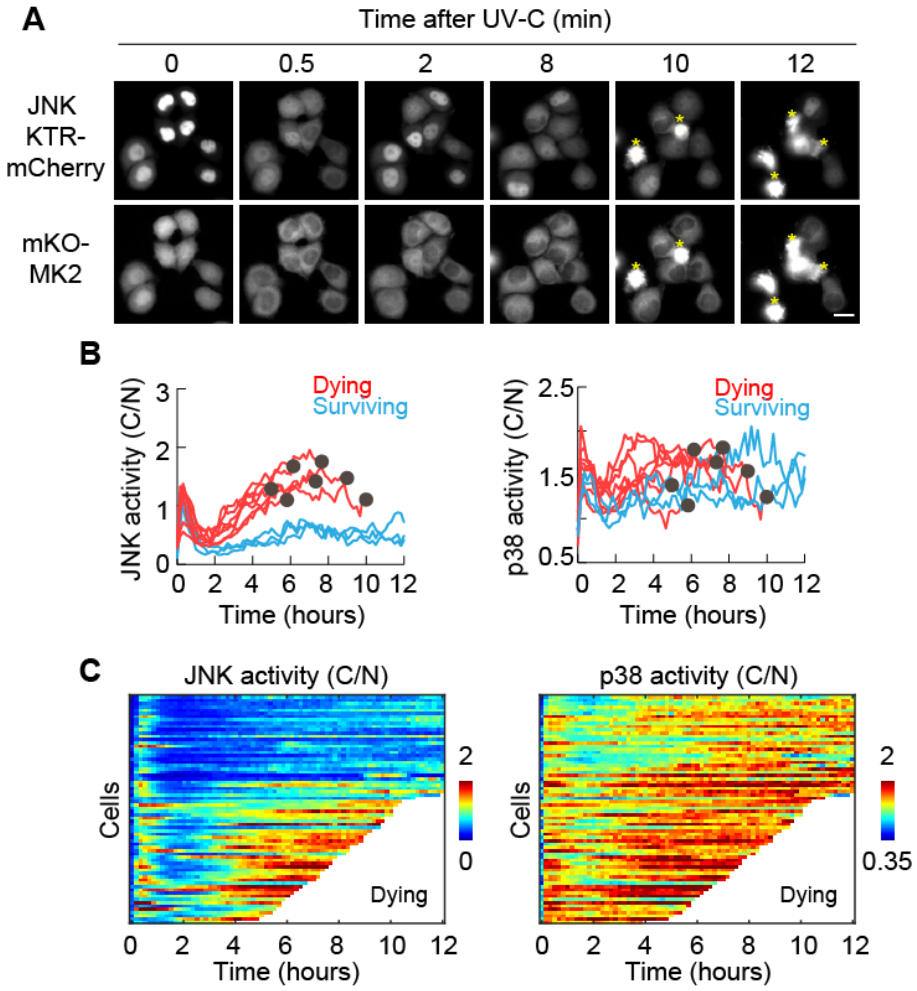

Figure 21. Cell-to-cell variation in JNK activity leads to fractional killing upon UV-C treatment.
(A) Representative images of clonal HeLa reporter cells, which were irradiated with 100 J/m^2 UV-C. Yellow asterisks indicate apoptotic cells. Scale bar: 20 µm.
(B) Timecourses of JNK KTR-mCherry and mKO-MK2 C/N ratios upon 100 J/m^2 UV-C stimulation for dying (red lines) and surviving (blue lines) cells from (A). Black dots indicate apoptosis. n = 10 representative cells.
(C) Heatmaps of JNK KTR-mCherry and mKO-MK2 C/N ratios for cells from (A). White traces indicate cells that underwent cell death. n = 70 cells from four independent experiments.

For this purpose, clonal HeLa reporter cells were irradiated with 100 J/m^2 UV-C, followed by observation of JNK, p38 activities and cellular outcomes (survival and apoptosis) in single cells for 12 h (Figure 21A). Rapid and transient increase in JNK and p38 activities was observed within 30 min in both surviving and dying cells (Figure 21B). Strikingly, 2 h post UV-C exposure, JNK activity markedly increased again in the cells that were doomed to die (Figures 21B and 21C). Meanwhile, p38 activity also increased after 2 h, but did not show a significant difference between surviving and dying cells (Figures 21B and 21C). This was reproducible in MCF10A cells, which also showed elevated second phase JNK activities in the cells that were doomed to undergo apoptosis, but comparable p38 activities in surviving and dying cells (Figure 22).

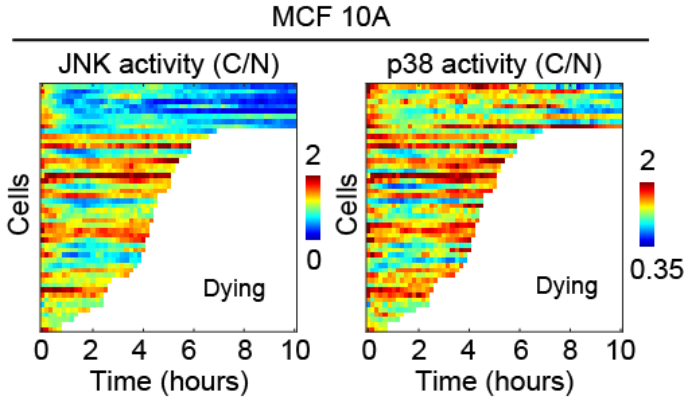

Figure 22. UV-C-induced JNK and p38 activities in MCF 10A cells.
Heatmaps of JNK KTR-mCherry and mKO-MK2 C/N ratios in NJP expressing MCF 10A after irradiation with 100 J/m^2 UV-C. n = 50 cells from two independent experiments.

The next aim was to determine which of p38 or JNK activities was correlated with cell death. For this, the average kinase activities of single cells in the initial phase (< 2 h) and later phase (> 4 h) were extracted from the time lapse data and compared between dying and surviving cells (Figure 23). As evident in the histograms, the mean JNK activities of the later phase were significantly associated with the dying cells (Figure 23A). The other three parameters, i.e. mean JNK activity in initial phase, mean p38 activity in initial phase, and mean p38 activity in later phase, did not significantly differ between dying and surviving cells (Figure 23A and 23B). Logistic regression analysis was conducted to assess the probability of cell death as a function of the mean JNK activity in the later phase. A threshold in JNK activity (C/N) of 0.68 was determined (Figure 23A, green curve).

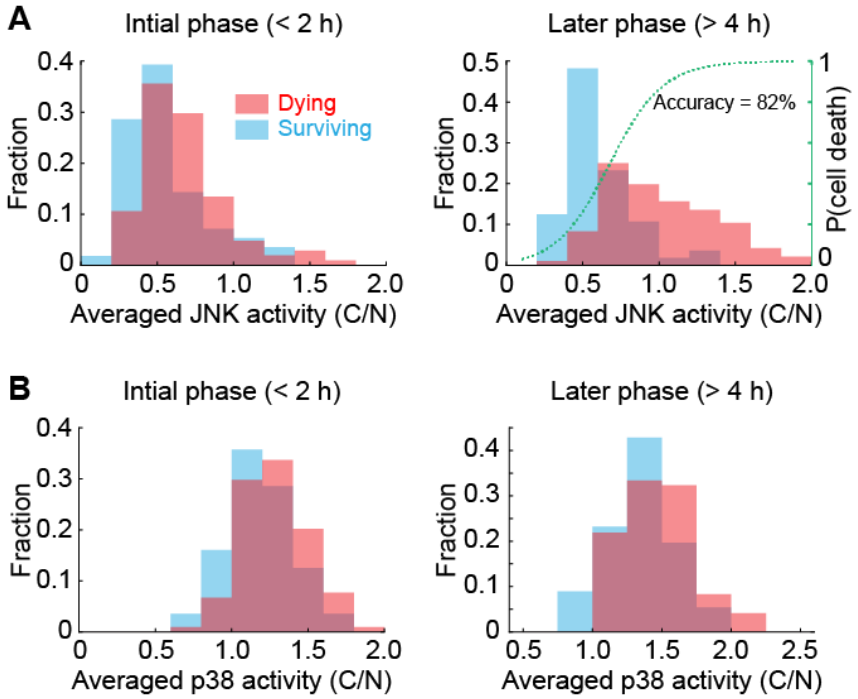

Figure 23. Later phase JNK activities are associated with cell death upon UV-C stimulation.
(A-B) Histograms of averaged JNK KTR-mCherry and mKO-MK2 C/N ratios in the initial phase (< 2 h) and later phase (> 4 h) after 100 J/m^2 UV-C stimulation are shown for dying (red) and surviving (blue) cells. The green dashed line represents the estimated probability of cell death as a function of JNK activity, which is obtained by the logistic regression. Data were analyzed by Dr. Yohei Kondo.

In line with previous studies (Chen et al., 1996; Staples et al., 2010; Tournier et al., 2000), JNK inhibitor pretreatment markedly prevented UV-C-induced apoptosis, confirming that JNK signaling has an essential role in the induction of apoptosis (Figure 24A). Of note, addition of JNK inhibitor 2 h after UV-C blocked apoptosis as much as pretreatment, implying that the later phase JNK activity is required for apoptosis, but not the initial peak in JNK activity (Figure 24B). (Chen et al., 1996)

To examine whether the long-term heterogeneity in JNK activity was also a result of p38-mediated suppression, I studied the effect of SB203580 on long-term JNK activity dynamics. Inhibition of p38 activity by SB203580 led to prolonged UV-induced JNK activities in single cells (Figures 24C and 24D), indicating that cross-inhibition of JNK activities by p38 originated the long-term cell-to-cell-variability in JNK activities. I predicted that sustained JNK activities by SB203580 treatment would result in higher apoptosis following UV-C, however, the fraction of apoptotic cells showed no difference between SB203580 and control pretreatments (Figure 24A). I reasoned, that p38 activation might also promote cell death, so that blocking of apoptosis-promoting effects by SB203580 would

neutralize the effect of increased JNK activity. Therefore, I looked for an approach to specifically stop the cross-inhibition of JNK without inhibiting p38 activity.

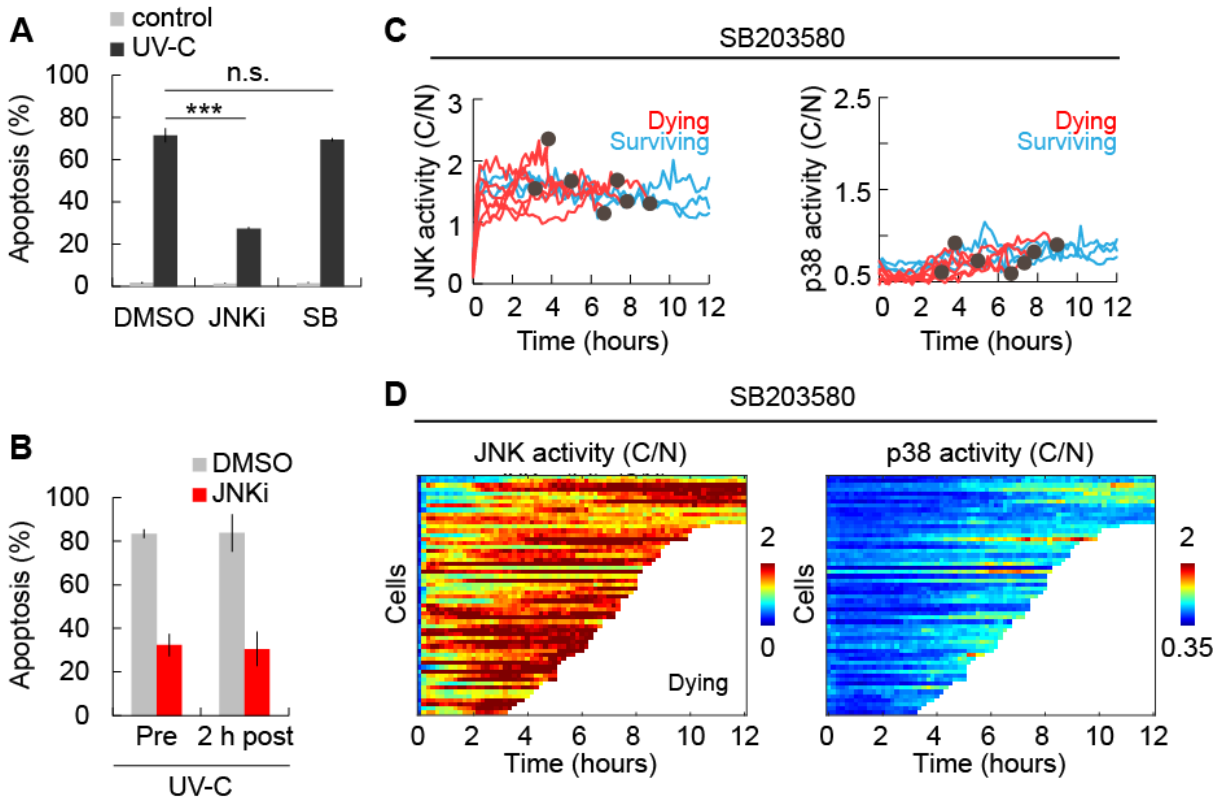

Figure 24. Role of JNK and p38 in UV-C induced cell death.
(A) Apoptosis of 0.1% DMSO, 10 µM JNK inhibitor VIII (JNKi), or 10 µM SB203580 (SB)-pretreated HeLa cells 12h after 100 J/m^2 UV-C or mock treatment. Data are shown as the mean with SD. n = 3 independent experiments.
(B) Apoptosis of 0.1% DMSO or 10 µM JNK inhibitor VIII (JNKi)-treated HeLa cells 12 h upon 100 J/m^2 UV-C. JNK inhibitor was added before (pre) or 2 h after UV-C irradiation. Data are shown as the mean with SD. n = 3 independent experiments.
(C) JNK KTR-mCherry and mKO-MK2 C/N ratios of 10 µM SB203580-pretreated clonal HeLa reporter cells are shown for dying (red lines) and surviving (blue lines) cells after 100 J/m^2 UV-C stimulation. Black dots indicate apoptosis. n = 10 representative cells.
(D) Heatmaps of JNK KTR-mCherry and mKO-MK2 C/N ratios of SB203580-pretreated cells from (C). n = 58 cells.

3-10 Efficiency of *DUSP1* induction determines cell fate after UV-C stress

As has already been demonstrated in Figure 15, DUSP1 depletion abrogates p38's transcriptional cross-inhibition of JNK. I adopted this approach to study the role of cross-inhibition of JNK in the cell death decision. *DUSP1* KO strongly potentiated and maintained JNK activity in every cell, compared to the control *RLuc* KO control cells, which did not

affect the heterogeneous JNK responses (Figure 25A). Importantly, *DUSP1* KO sensitized cells to UV-C-induced cell death, as evident from the increased fraction of apoptotic cells (>90%) and accelerated cell death (Figures 25B and 25C). JNK inhibition largely suppressed apoptosis of *DUSP1* KO cells, suggesting that the lethality of *DUSP1* KO cells was attributed to the increased JNK signaling (Figure 25B). SB203580 slightly, but significantly ameliorated apoptosis of *DUSP1* KO cells (Figure 25B), supporting the idea that p38 has two antagonistic roles in UV-C-induced cell death. On the one hand, p38 protects from apoptosis by repressing JNK activity via *DUSP1* induction, on the other hand p38 mildly promotes apoptosis in a manner independent of DUSP1.

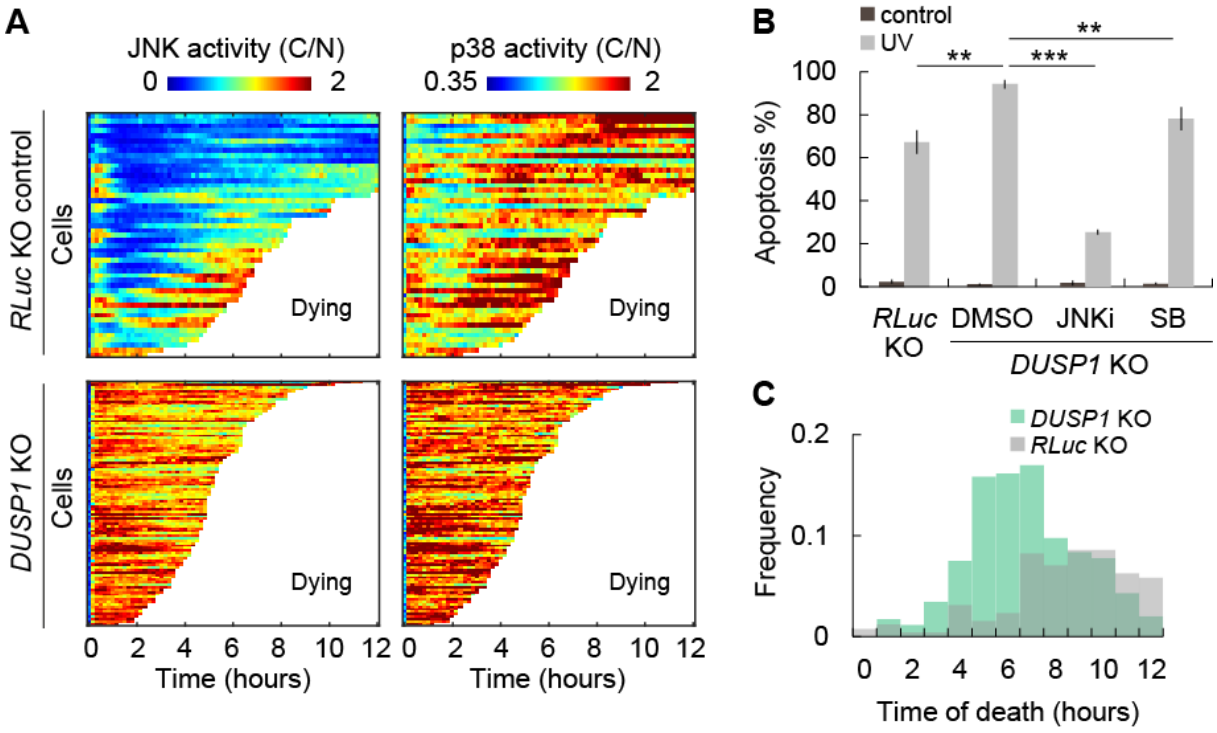

Figure 25. DUSP1 generates cell-to-cell heterogeneity of JNK activation and protects from cell death.
(A) Heatmaps of JNK KTR-mCherry and mKO-MK2 C/N ratios in NJP expressing HeLa *DUSP1* KO and *RLuc* KO control cells upon 100 J/m^2 UV-C. n = 49 cells for *RLuc* KO and n = 100 cells for *DUSP1* KO.
(B) Apoptosis of 0.1% DMSO, 10 µM JNK inhibitor VIII (JNKi), 10 µM SB203580 (SB)-pretreated *DUSP1* KO cells and *RLuc* KO control cells 12 h after 100 J/m^2 UV-C or mock treatment. Data are shown as the mean with SD. n = 3 independent experiments.
(C) Histogram of the time duration till cell death of *DUSP1* KO and *RLuc* KO HeLa cells upon 100 J/m^2 UV-C treatment, determined by live-cell microscopy. n = 255 cells for *RLuc* KO and n = 347 cells for *DUSP1* KO.

These data point to the hypothesis that variability in p38-induced DUSP1 levels might be a source for the cell-to-cell heterogeneity of JNK activity. First, I confirmed that UV-C irradiation induced *DUSP1* mRNA expression with a peak at 2 h and that this induction was dependent on p38 activity (Figure 26A). To track single cell DUSP1 protein levels, I

knocked-in *mScarlet* to the 3'end of *DUSP1* gene by CRISPR/Cas9-mediated gene transfer (Figure 26B). For positive and negative selections, a loxP-flanked dTKneo selection cassette was attached to mScarlet via a P2A sequence and at a later step eliminated by Cre-mediated recombination (Figure 26B). Western blot analysis of clonal DUSP1-mScarlet knock-in cells before Cre expression detected a band corresponding to the size of DUSP1-mScarlet of 68 kDa (Figure 26C). Notably, these bands could not be observed after removal of the dTKneo cassette (Figure 26C). The drop of expression after removal of the selection cassette is reasonable, since *DUSP1* is usually not expressed in the basal state, and suggests a role of 3'UTR of *DUSP1* gene in the mRNA stability. Importantly, UV-C stress led to an increase in mScarlet fluorescence in a fraction of cells (Figure 26D). The DUSP1-mScarlet fluorescence started to rise behind *DUSP1* mRNA, which is possibly due to the slow maturation of mScarlet (Bindels et al., 2017). To analyze the relationship between DUSP1 levels and JNK activity, JNK KTR-Clover was co-expressed in DUSP1-mScarlet knock-in cells. The induction of DUSP1-mScarlet was heterogeneous among cells and, strikingly, cells with high DUSP1-mScarlet levels exhibited low JNK activity (Figure 26E). Plotting single cell JNK activities versus DUSP1 levels revealed a negative correlation between JNK activities and DUSP1 levels (Figure 26F). Furthermore, the cells that induced DUSP1-mScarlet expression survived after the UV-C treatment, while the cells without DUSP1-mScarlet induction exhibited apoptosis (Figure 26G).

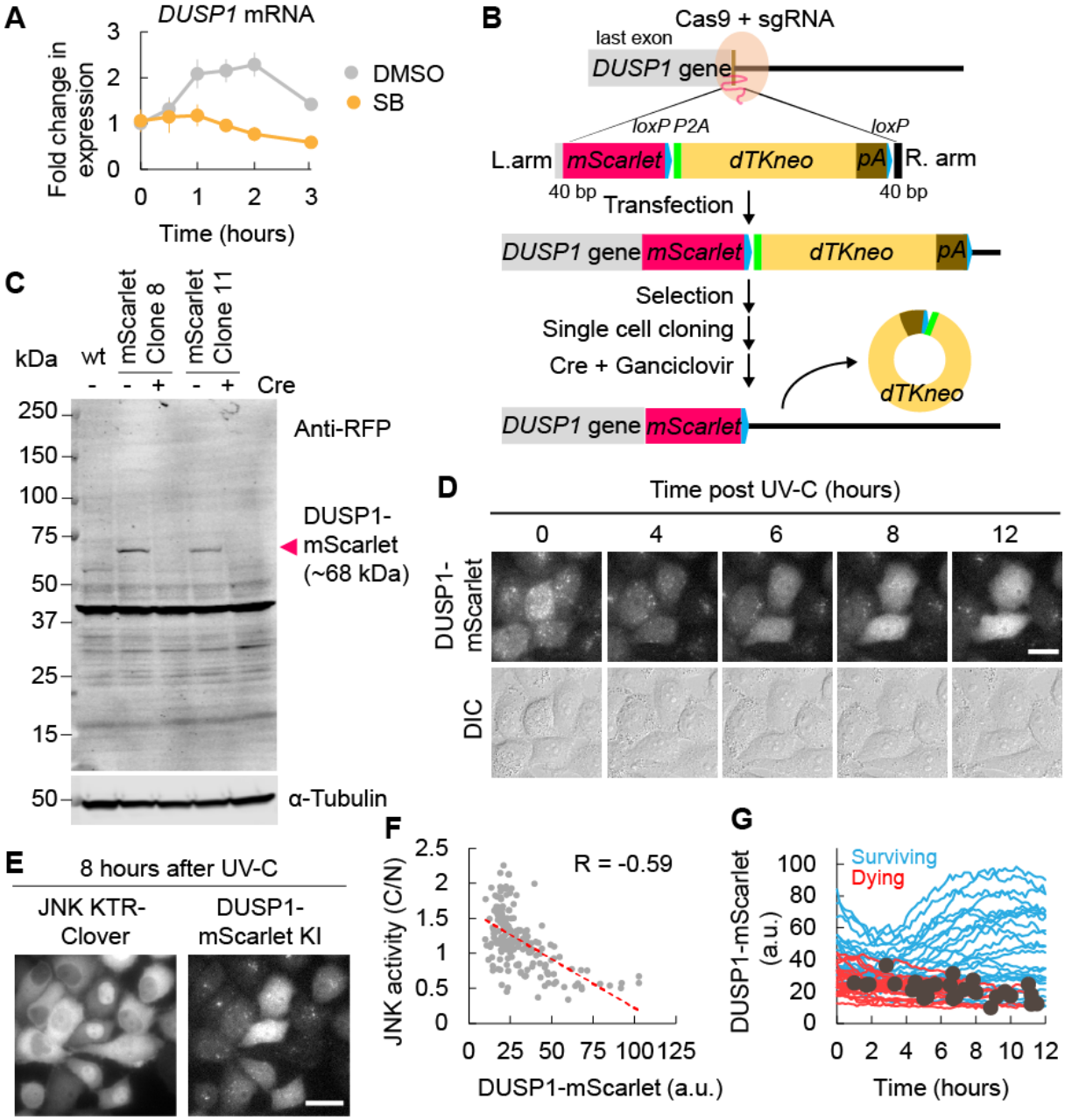

Figure 26. DUSP1 levels negatively correlate with JNK activity.

(A) Fold changes of *DUSP1* mRNA levels of 0.1% DMSO or 10 µM SB203580 (SB)-pretreated HeLa cells after 100 J/m^2 UV-C. Data are shown as mean with SD. n = 3 independent experiments.

(B) Scheme of the DUSP1-mScarlet knock-in method.

(C) Western blot analysis of HeLa DUSP1-mScarlet KI clones 8 and 11 before and after AAV-Cre infection.

(D) Representative images of HeLa DUSP1-mScarlet KI cells (clone 8) after stimulation with 100 J/m^2 UV-C. Scale bar: 20 µm.

(E) Representative images of JNK KTR-Clover expressing HeLa DUSP1-mScarlet KI cells are shown at 8 h 20 min after 100 J/m^2 UV-C treatment. Scale bar: 30 µm.

(F) Negative correlation of single cell JNK KTR-Clover C/N ratios with DUSP1-mScarlet levels at 8 hours 20 min after 100 J/m^2 UV-C exposure. n = 200 cells from two independent experiments. The Pearson correlation value R was obtained by linear regression.

(G) Time courses of DUSP1-mScarlet for dying (red lines) and surviving (blue lines) cells after stimulation with 100 J/m^2 UV-C. Black dots indicate apoptosis. n = 54 cells from two independent experiments.

In conclusion, I propose that in response to UV-C stress, fluctuation in p38-induced *DUSP1* gene induction generates cell-to-cell heterogeneity in JNK activity and determines the cell fate decision, survival or cell death, leading to fractional killing. Loss of cross-inhibition by p38 would result in excessive JNK activities above the threshold and cause complete cell death (Figure 27).

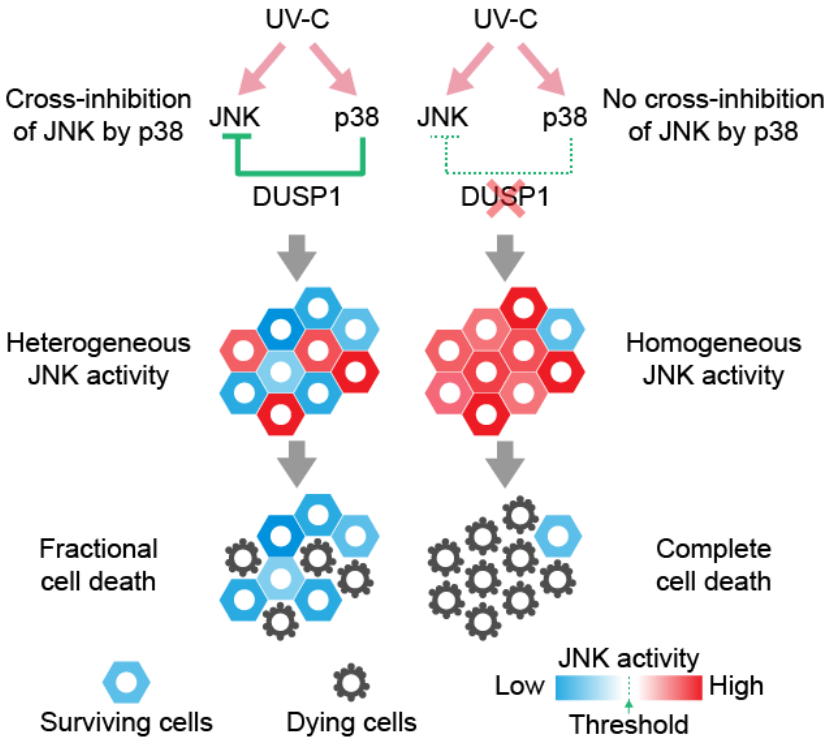

Figure 27. Cross-inhibition by p38 causes cell-to-cell variability of stress-induced JNK activities which determines life-death decisions.
Cross-inhibition of JNK by p38-induced DUSP1 expression generates heterogeneity in JNK activity upon UV-C stress and leads to fractional killing (left). In absence of DUSP1-mediated cross-inhibition, increased JNK activities would lead to complete cell death (right).

Chapter 4

Discussion and Conclusion

In this study, I established a highly specific and sensitive multiplexed imaging system for JNK and p38 activities, which enables simultaneous visualization of two kinase activities in living cells at single-cell resolution. This imaging system provides a potent tool to quantitatively investigate the crosstalk of JNK and p38 kinases. Tracking the signaling dynamics in diverse stress and inflammatory conditions and targeted perturbations of SAPK activity by pharmacological and genetic manipulations provided compelling evidence that p38 signaling antagonizes JNK activity through both post-translational and transcriptional mechanisms with the relative strength of each pathway depending on the stimulant. With respect to molecular mechanisms, I could confirm and expand the idea that TAB1/TAK1 and *DUSP1* gene expression were involved in post-translational and transcriptional cross-inhibition of JNK, respectively. To take full advantage of my imaging system, I performed multiplexed live cell imaging, and strikingly, revealed that p38-mediated cross-inhibition of JNK generated remarkable cell-to-cell heterogeneity in JNK activity. Analysis of endogenous DUSP1 protein levels strongly suggests that variability in *DUSP1* expression causes the cell-to-cell heterogeneity in JNK activity. Finally, I found that this cell-to-cell heterogeneity in JNK activity not only correlated with, but also caused fractional killing in response to UV-C stress. Therefore, I can infer that p38-mediated cross-inhibition of JNK determines the cell fate decision between survival and cell death in response to UV-C stress.

The findings of this work are in good agreement with previous cell population-based studies that p38 suppresses JNK signaling in diverse cellular contexts (Caballero-Franco et al., 2013; Cheung et al., 2003; Heinrichsdorff et al., 2008; Hui et al., 2007; Jones et al., 2018; Kim et al., 2008; Staples et al., 2010). While most of these reports described cross-inhibition in a specific cell type and stimulatory condition, this study expands that view by the quantitative evaluation of post-translational and transcriptional mechanisms under various stress and inflammatory stimuli (Figure 14D). Thus, this study suggests that multiple mechanisms cooperate to keep JNK activity in check, while the relative strength of these cross-inhibition mechanisms is dependent on the type of stimulant. Here, I have described cross-inhibition of JNK by p38 upon five different stimuli. Furthermore, I have also shown an inverse correlation between JNK and p38 activities during cell cycle progression in the absence of any stimuli. I have observed minimal JNK and relatively high p38 activities in the first half of cell cycle and increasing JNK and minimal p38 activities in the second half of cell cycle (Figure 10). It is tempting to speculate that p38's cross-inhibition of JNK also operates in the absence of any stimuli, but this remains to be determined.

As an example of post-translational cross-inhibition, Cheung *et al.* proposed that in response to pro-inflammatory cytokines and osmotic stress, p38 mediates negative feedback control of TAK1 and downstream kinases by phosphorylating TAB1 on Ser423 and Thr431 (Cheung et al., 2003). My results support this model in that the rescue experiment with the non-phosphorylatable TAB1 mutant further increased JNK activity upon stimulation with TNFα and IL-1β (Figure 16D). However, as opposed to the model of negative feedback, this non-phosphorylatable TAB1 mutant did not affect p38 activity itself (Figure 16E). As a matter of fact, Cheung *et al.* carefully characterized TAB1 phosphorylation, TAK1 activity, and JNK activation, but did not show p38 activation (Cheung et al., 2003). One possible explanation for this finding is that TAB1 is essential for TAK1 activity towards JNK, but not p38 in HeLa cells. This is supported by the observation that TNFα-induced JNK activation was completely impaired in *TAB1* and *TAK1* KO cells, whereas TNFα-induced p38 activation not changed in *TAB1* KO cells (Figures 16D and 16E). Another possible explanation is that a p38-specific MAPKKK may compensate for the p38 activation. In fact, it has been reported that TAO2, a MAPKKK that preferentially activates the p38 pathway, is activated by sorbitol-induced osmotic stress (Chen and Cobb, 2001).

As for transcriptional inhibition of JNK, it is well documented that p38 can induce expression of DUSP1, a phosphatase of JNK and p38, in response to various stresses and inflammatory stimuli (Ferreiro et al., 2010; Kim et al., 2008; Staples et al., 2010; Tomida et al., 2015). In line with these studies, *DUSP1* KO prolonged and potentiated JNK activity in response to anisomycin and UV-C stress (Figure 15D and 15E). However, it is elusive why DUSP1 hardly inactivated p38 in my system, when cells were treated with anisomycin and UV-C (Figure 5D and 15E). This observation could possibly be explained by substrate preference of DUSP1 for JNK over p38. In this regard, it has been reported that DUSP1 binds to JNK1 with higher affinity than to p38α, which is paralleled with higher catalytic activation of DUSP1 (Slack et al., 2001). In line with my data, a previous study demonstrated that UV-C-stimulated JNK phosphorylation is quickly downregulated in MEFs within 90 min, concomitant with DUSP1 induction, while p38 phosphorylation decreases with much slower kinetics, with some level remaining up to 6 h after UV-C irradiation (Staples et al., 2010).

Taken together, neither TAB1 phosphorylation in the case of TNFα and IL-1β, nor *DUSP1* induction in the case of anisomycin and UV-C downregulate p38 activity efficiently, although two mechanisms inactivate JNK, as demonstrated by multiplexed imaging (Figures 15D, 15E, 16D, and 16E). In support of our imaging results, also p38 inhibition did not affect

the level of endogenous p38 phosphorylation itself, as demonstrated by western blot analysis (Figure 12A). These results challenge the previous view of negative feedback control of SAPK signaling by p38 and instead suggest a model of cross-inhibition, in which p38 rather specifically suppresses JNK activation, but not its own activation.

One of the key findings of this study is that cross-inhibition by p38 generates cell-to-cell variability in JNK activity. I found that this principle is applicable to many different inflammatory and stress conditions (Figure 17E) and a broad range of different cell lines (Figure 19). In contrast, the cell-to-cell variation of p38 remains constant upon stimulation (Figures 17B and 18). Interestingly, high-content imaging of multiple signaling pathways based on FRET biosensors demonstrated that CV of single cell JNK activities after EGF stimulation was by far the highest among more than 15 key signaling nodes, such as EGFR, Ras, Rac, ERK, Akt, and so on (Kuchenov et al., 2016), implying that cell-to-cell heterogeneity in JNK activity may be exceptionally high compared to other signaling pathways.

What is the biological relevance of cross-inhibition and heterogeneity of JNK signaling? Here, I exemplified the importance of p38-mediated cross-inhibition and resulting heterogeneity in JNK activity with fractional killing in response to UV-C. Staples *et al.* reported in their cell-population study that p38-induced *DUSP1* protects MEFs from UV-C-induced apoptosis by inactivating JNK (Staples et al., 2010). My imaging system supports this finding and has further revealed that UV-C stress leads to variable JNK activation at the single cell level and that this heterogeneity in JNK activity is significantly associated with the cell fate of survival or death (Figure 21). In particular, cells with low JNK activity in later phase survived, while cells with higher JNK activity underwent apoptosis, implying the existence of a critical threshold of JNK activity for the execution of apoptosis (Figure 23). My data provided evidence that cell-to-cell variability in p38-induced *DUSP1* expression caused heterogeneous JNK activity after UV-C stress and thereby governed the cell fate (Figures 25 and 26). Blocking this cross-inhibition leads to aberrantly high JNK activation above the threshold and thereby to cell death (Figure 25). Thus, DUSP1-mediated cross-inhibition of JNK seems to be crucial to protect the cells from UV-C stress-induced apoptosis.

As mentioned above, cell-to-cell variability of *DUSP1* induction causes cell-to-cell variability of JNK activity. However, how *DUSP1* induction varies between cells remains elusive. It is proposed that the intrinsic noise of gene expression results in variability in the abundance of proteins across a cell population and in the same cell over time, which is known

as non-genetic heterogeneity and can eventually lead to resistance or persistence to anticancer drugs or antibiotics at the population level (Brock et al., 2009; Wakamoto et al., 2013). It is therefore possible that plasticity in the cellular state or noise in the stress-induced gene expression might have led to the variability in DUSP1 expression levels. According to this mechanism, it is plausible that the heterogeneity in cross-inhibition of JNK by p38 confers resistance to cells against stress stimuli. On the other hand, it is unknown how post-translational cross-inhibition by p38 generates heterogeneity in JNK activity and whether it is linked to cellular outcomes. Future work is needed to elucidate the degree to which the cross-inhibition via p38 contributes to the heterogeneous JNK activity, and the mechanism underlying this effect.

Intriguing studies using mouse models of conditional p38α KO have demonstrated that p38-mediated cross-regulation of JNK is crucial for tissue homeostasis. For example, *p38α* KO leads via aberrant JNK activity to excessive proliferation and inadequate differentiation in the intestine, skin, and liver and make those tissues prone to damage and environmental insults (Caballero-Franco et al., 2013; Heinrichsdorff et al., 2008; Hui et al., 2007). In some cases, *p38α* KO can even promote tumor development by upregulation of the JNK pathway (Hui et al., 2007). These studies let us speculate that heterogeneity in JNK activity, e.g. after EGF stimulation, might also regulate the cell fate decision whether to proliferate or not. It would also be interesting to explore in future studies, whether heterogeneity in p38-mediated cross-inhibition of JNK exists *in vivo* and whether it plays a role in tissue vulnerability and homeostasis.

Targeting p38-mediated suppression of JNK could potentially be beneficial for combination anticancer therapy. Since p38 inhibition turned fractional to complete killing of cells after DNA-damaging UV-C irradiation, p38 inhibition has potential to be used in combination with DNA damage-inducing chemotherapeutic drugs to increase their efficacy. In fact, it has been reported that p38 inhibition potentiated the anti-leukemic activity of Smac mimetics, via JNK mediated upregulation of TNF production (Lalaoui et al., 2016). Furthermore, inhibition of p38 sensitizes tumor cells to cisplatin-induced apoptosis by activating the JNK pathway (Pereira et al., 2013). Since the timing and the order of drug administration can affect the efficacy of the combinatorial therapy due to rewiring of specific signaling pathways (Chen et al., 2016; Lee et al., 2012), it would first of all be crucial to examine how p38 inhibition affects JNK signaling pathway and sensitivity to drugs. Our imaging system provides a suitable platform to quantitatively understand the effect of p38 inhibition and its timing on drug-induced JNK signaling dynamics and cell death.

Our imaging system is based on KTRs, which enabled multiplexed imaging of the signaling dynamics of the three MAPKs ERK, JNK, and p38 in single cells (Regot et al., 2014). Since the p38 KTR reporter showed limited nucleo-cytoplasmic shuttling, here I took advantage of the naturally shuttling p38 substrate MK2 as a live-cell imaging reporter for p38 activity, which showed higher sensitivity than p38 KTR. This translocation of MK2 has been used for screening p38 inhibitors (Anton et al., 2014; Trask et al., 2006). Exogenous expression of MK2 had no obvious effect on the phenotype of HeLa cells during their maintenance and cell death studies; however, it remains to be examined whether MK2 overexpression perturbs the signaling and affects the phenotype of the cells of interest. Nevertheless, this highly sensitive and specific multiplexed imaging system will be useful to quantitatively evaluate the complex crosstalk of JNK and p38, reveal the heterogeneity of their interaction among single cells, and ultimately study the role of their signaling dynamics in phenotypic outcomes.

Bibliography

Albeck, J.G., Burke, J.M., Aldridge, B.B., Zhang, M., Lauffenburger, D. a., and Sorger, P.K. (2008). Quantitative Analysis of Pathways Controlling Extrinsic Apoptosis in Single Cells. Mol. Cell *30*, 11–25.

Ambrosino, C., and Nebreda, A.R. (2001). Cell cycle regulation by p38 MAP kinases. Biol. Cell *93*, 47–51.

Ananieva, O., Darragh, J., Johansen, C., Carr, J.M., McIlrath, J., Park, J.M., Wingate, A., Monk, C.E., Toth, R., Santos, S.G., et al. (2008). The kinases MSK1 and MSK2 act as negative regulators of Toll-like receptor signaling. Nat. Immunol. *9*, 1028–1036.

Anton, R., Bauer, S.M., Keck, P.R.W.E.F., Laufer, S., and Rothbauer, U. (2014). A p38 substrate-specific MK2-EGFP translocation assay for identification and validation of new p38 inhibitors in living cells: a comprising alternative for acquisition of cellular p38 inhibition data. PLoS One *9*, e95641.

Aoki, K., Kumagai, Y., Sakurai, A., Komatsu, N., Fujita, Y., Shionyu, C., Matsuda, M., Hou, C., Li, L., Qin, Z.S., et al. (2013). Stochastic ERK activation induced by noise and cell-to-cell propagation regulates cell density-dependent proliferation. Mol. Cell *52*, 529–540.

Arthur, J.S.C., and Ley, S.C. (2013). Mitogen-activated protein kinases in innate immunity. Nat. Rev. Immunol. *13*, 679–692.

Bindels, D.S., Haarbosch, L., van Weeren, L., Postma, M., Wiese, K.E., Mastop, M., Aumonier, S., Gotthard, G., Royant, A., Hink, M.A., et al. (2017). mScarlet: a bright monomeric red fluorescent protein for cellular imaging. Nat. Methods *14*, 53–56.

Bode, A.M., and Dong, Z. (2007). The functional contrariety of JNK. Mol. Carcinog. *46*, 591–598.

Brinkman, E.K., Chen, T., Amendola, M., and Van Steensel, B. (2014). Easy quantitative assessment of genome editing by sequence trace decomposition. Nucleic Acids Res. *42*, 1–8.

Brock, A., Chang, H., and Huang, S. (2009). Non-genetic heterogeneity--a mutation-independent driving force for the somatic evolution of tumours. Nat. Rev. Genet. *10*, 336–342.

Bulavin, D.V., Saito, S., Hollander, M.C., Sakaguchi, K., Anderson, C.W., Appella, E., and Fornace, A.J., Jr (1999). Phosphorylation of human p53 by p38 kinase coordinates N-terminal phosphorylation and apoptosis in response to UV radiation. EMBO J. *18*, 6845–6854.

Bulavin, D.V., Higashimoto, Y., Popoff, I.J., Gaarde, W.A., Basrur, V., Potapova, O., Appella, E., and Fornace, A.J., Jr (2001). Initiation of a G2/M checkpoint after ultraviolet radiation requires p38 kinase. Nature *411*, 102–107.

Caballero-Franco, C., Choo, M.-K., Sano, Y., Ritprajak, P., Sakurai, H., Otsu, K., Mizoguchi, A., and Park, J.M. (2013). Tuning of protein kinase circuitry by p38α is vital for epithelial tissue homeostasis. J. Biol. Chem. *288*, 23788–23797.

Cai, B., Chang, S.H., Becker, E.B.E., Bonni, A., and Xia, Z. (2006). p38 MAP kinase mediates apoptosis through phosphorylation of BimEL at Ser-65. J. Biol. Chem. *281*, 25215–25222.

Casanovas, O., Miró, F., Estanyol, J.M., Itarte, E., Agell, N., and Bachs, O. (2000). Osmotic stress regulates the stability of cyclin D1 in a p38SAPK2-dependent manner. J. Biol. Chem. *275*, 35091–35097.

Chen, Z., and Cobb, M.H. (2001). Regulation of Stress-responsive Mitogen-activated Protein (MAP) Kinase Pathways by TAO2. J. Biol. Chem. *276*, 16070–16075.

Chen, S.-H., Forrester, W., and Lahav, G. (2016). Schedule-dependent interaction between anticancer treatments. Science *351*, 1204–1209.

Chen, Y.R., Wang, X., Templeton, D., Davis, R.J., and Tan, T.H. (1996). The role of c-Jun N-terminal kinase (JNK) in apoptosis induced by ultraviolet C and gamma radiation. Duration of JNK activation may determine cell death and proliferation. J. Biol. Chem. *271*, 31929–31936.

Cheung, P.C.F., Campbell, D.G., Nebreda, A.R., and Cohen, P. (2003). Feedback control of the protein kinase TAK1 by SAPK2a/p38alpha. EMBO J. *22*, 5793–5805.

Chi, H., Barry, S.P., Roth, R.J., Wu, J.J., Jones, E.A., Bennett, A.M., and Flavell, R.A. (2006). Dynamic regulation of pro- and anti-inflammatory cytokines by MAPK phosphatase 1 (MKP-1) in innate immune responses. Proc. Natl. Acad. Sci. U. S. A. *103*, 2274–2279.

Cuadrado, A., and Nebreda, A.R. (2010). Mechanisms and functions of p38 MAPK signalling. Biochem. J. *429*, 403–417.

Cuenda, A., and Rousseau, S. (2007). p38 MAP-kinases pathway regulation, function and role in human diseases. Biochim. Biophys. Acta *1773*, 1358–1375.

Cuevas, B.D., Abell, A.N., and Johnson, G.L. (2007). Role of mitogen-activated protein kinase kinase kinases in signal integration. Oncogene *26*, 3159–3171.

Deak, M., Clifton, A.D., Lucocq, L.M., and Alessi, D.R. (1998). Mitogen- and stress-activated protein kinase-1 (MSK1) is directly activated by MAPK and SAPK2/p38, and may mediate activation of CREB. EMBO J. *17*, 4426–4441.

Dérijard, B., Hibi, M., Wu, I.H., Barrett, T., Su, B., Deng, T., Karin, M., and Davis, R.J. (1994). JNK1: A protein kinase stimulated by UV light and Ha-Ras that binds and phosphorylates the c-Jun activation domain. Cell *76*, 1025–1037.

Durandau, E., Aymoz, D., and Pelet, S. (2015). Dynamic single cell measurements of kinase activity by synthetic kinase activity relocation sensors. BMC Biol. *13*, 55.

Engel, K., Kotlyarov, A., and Gaestel, M. (1998). Leptomycin B-sensitive nuclear export of MAPKAP kinase 2 is regulated by phosphorylation. EMBO J. *17*, 3363–3371.

Ferreiro, I., Joaquin, M., Islam, A., Gomez-Lopez, G., Barragan, M., Lombardía, L., Domínguez, O., Pisano, D.G., Lopez-Bigas, N., Nebreda, A.R., et al. (2010). Whole genome analysis of p38 SAPK-mediated gene expression upon stress. BMC Genomics *11*, 144.

Fosbrink, M., Aye-Han, N.-N., Cheong, R., Levchenko, A., and Zhang, J. (2010). Visualization of JNK activity dynamics with a genetically encoded fluorescent biosensor. Proc. Natl. Acad. Sci. U. S. A. *107*, 5459–5464.

Fuchs, S.Y., Adler, V., Pincus, M.R., and Ronai, Z. (1998). MEKK1/JNK signaling stabilizes and activates p53. Proc. Natl. Acad. Sci. U. S. A. *95*, 10541–10546.

Gaestel, M. (2006). MAPKAP kinases - MKs - two's company, three's a crowd. Nat. Rev. Mol. Cell Biol. *7*, 120–130.

Gupta, S., Campbell, D., Dérijard, B., and Davis, R.J. (1995). Transcription factor ATF2 regulation by the JNK signal transduction pathway. Science *267*, 389–393.

Gutierrez, G.J., Tsuji, T., Chen, M., Jiang, W., and Ronai, Z.A. (2010). Interplay between Cdh1 and JNK activity during the cell cycle. Nat. Cell Biol. *12*, 686–695.

Hammer, M., Mages, J., Dietrich, H., Servatius, A., Howells, N., Cato, A.C.B., and Lang, R. (2006). Dual specificity phosphatase 1 (DUSP1) regulates a subset of LPS-induced genes and protects mice from lethal endotoxin shock. J. Exp. Med. *203*, 15–20.

Han, J., Jiang, Y., Li, Z., Kravchenko, V.V., and Ulevitch, R.J. (1997). Activation of the transcription factor MEF2C by the MAP kinase p38 in inflammation. Nature *386*, 296–299.

Hao, N., Budnik, B.A., Gunawardena, J., and O'Shea, E.K. (2013). Tunable signal processing through modular control of transcription factor translocation. Science *339*, 460–464.

Heinrichsdorff, J., Luedde, T., Perdiguero, E., Nebreda, A.R., and Pasparakis, M. (2008). p38 alpha MAPK inhibits JNK activation and collaborates with IkappaB kinase 2 to prevent endotoxin-induced liver failure. EMBO Rep. *9*, 1048–1054.

Hibi, M., Lin, A., Smeal, T., Minden, A., and Karin, M. (1993). Identification of an oncoprotein- and UV-responsive protein kinase that binds and potentiates the c-Jun activation domain. Genes Dev. *7*, 2135–2148.

Holohan, C., Van Schaeybroeck, S., Longley, D.B., and Johnston, P.G. (2013). Cancer drug resistance: an evolving paradigm. Nat. Rev. Cancer *13*, 714–726.

Hui, L., Bakiri, L., Mairhorfer, A., Schweifer, N., Haslinger, C., Kenner, L., Komnenovic, V., Scheuch, H., Beug, H., and Wagner, E.F. (2007). p38alpha suppresses normal and cancer cell proliferation by antagonizing the JNK-c-Jun pathway. Nat. Genet. *39*, 741–749.

Johnson, G.L., and Lapadat, R. (2002). Mitogen-activated protein kinase pathways mediated by ERK, JNK, and p38 protein kinases. Science *298*, 1911–1912.

Jones, D.S., Jenney, A.P., Joughin, B.A., Sorger, P.K., and Lauffenburger, D.A. (2018). Inflammatory but not mitogenic contexts prime synovial fibroblasts for compensatory signaling responses to p38 inhibition. Sci. Signal. *11*.

Kawakami, K., and Noda, T. (2004). Transposition of the Tol2 Element, an Ac-Like Element from the Japanese Medaka Fish Oryzias latipes, in Mouse Embryonic Stem Cells. Genetics *166*, 895–899.

Kim, B.-J., Ryu, S.-W., and Song, B.-J. (2006). JNK- and p38 kinase-mediated phosphorylation of Bax leads to its activation and mitochondrial translocation and to apoptosis of human hepatoma HepG2 cells. J. Biol. Chem. *281*, 21256–21265.

Kim, C., Sano, Y., Todorova, K., Carlson, B.A., Arpa, L., Celada, A., Lawrence, T., Otsu, K., Brissette, J.L., Arthur, J.S.C., et al. (2008). The kinase p38 alpha serves cell type-specific inflammatory functions in skin injury and coordinates pro- and anti-inflammatory gene expression. Nat. Immunol. *9*, 1019–1027.

Komatsu, N., Aoki, K., Yamada, M., Yukinaga, H., Fujita, Y., Kamioka, Y., and Matsuda, M. (2011). Development of an optimized backbone of FRET biosensors for kinases and GTPases. Mol. Biol. Cell *22*, 4647–4656.

Komatsubara, A.T., Matsuda, M., and Aoki, K. (2017). Single-cell quantification of the concentration and dissociation constant of endogenous proteins. bioRxiv *236422*.

Komeili, A., and O'Shea, E.K. (1999). Roles of phosphorylation sites in regulating activity of the transcription factor Pho4. Science *284*, 977–980.

Kuchenov, D., Laketa, V., Stein, F., Salopiata, F., Klingmüller, U., and Schultz, C. (2016). High-Content Imaging Platform for Profiling Intracellular Signaling Network Activity in Living Cells. Cell Chem. Biol. *23*, 1550–1559.

Lalaoui, N., Hänggi, K., Brumatti, G., Chau, D., Nguyen, N.-Y.N., Vasilikos, L., Spilgies, L.M., Heckmann, D.A., Ma, C., Ghisi, M., et al. (2016). Targeting p38 or MK2 Enhances the Anti-Leukemic Activity of Smac-Mimetics. Cancer Cell *29*, 145–158.

Lee, M.J.J., Ye, A.S.S., Gardino, A.K.K., Heijink, A.M.M., Sorger, P.K.K., MacBeath, G., and Yaffe, M.B.B. (2012). Sequential Application of Anticancer Drugs Enhances Cell Death by Rewiring Apoptotic Signaling Networks. Cell *149*, 780–794.

Levine, J.H., Lin, Y., and Elowitz, M.B. (2013). Functional roles of pulsing in genetic circuits. Science *342*, 1193–1200.

Li, Y., Roberts, J., AkhavanAghdam, Z., and Hao, N. (2017). Mitogen-activated protein kinase (MAPK) dynamics determine cell fate in the yeast mating response. J. Biol. Chem. *292*, 20354–20361.

MacCorkle, R.A., and Tan, T.-H. (2005). Mitogen-activated protein kinases in cell-cycle control. Cell Biochem. Biophys. *43*, 451–461.

Marshall, C.J. (1995). Specificity of receptor tyrosine kinase signaling: transient versus sustained extracellular signal-regulated kinase activation. Cell *80*, 179–185.

Maryu, G., Matsuda, M., and Aoki, K. (2016). Multiplexed fluorescence imaging of ERK and Akt activities and cell-cycle progression. Cell Struct. Funct. *92*, 81–92.

Maryu, G., Miura, H., Uda, Y., Komatsubara, A.T., Matsuda, M., and Aoki, K. (2018). Live-cell Imaging with Genetically Encoded Protein Kinase Activity Reporters. Cell Struct. Funct. *43*, 61–74.

McLaughlin, M.M., Kumar, S., McDonnell, P.C., Van Horn, S., Lee, J.C., Livi, G.P., and

Young, P.R. (1996). Identification of mitogen-activated protein (MAP) kinase-activated protein kinase-3, a novel substrate of CSBP p38 MAP kinase. J. Biol. Chem. *271*, 8488–8492.

Mendoza, H., Campbell, D.G., Burness, K., Hastie, J., Ronkina, N., Shim, J.-H., Arthur, J.S.C., Davis, R.J., Gaestel, M., Johnson, G.L., et al. (2008). Roles for TAB1 in regulating the IL-1-dependent phosphorylation of the TAB3 regulatory subunit and activity of the TAK1 complex. Biochem. J. *409*, 711–722.

Meng, W., Swenson, L.L., Fitzgibbon, M.J., Hayakawa, K., Haar, E.T., Behrens, A.E., Fulghum, J.R., and Lippke, J. a. (2002). Structure of mitogen-activated protein kinase-activated protein (MAPKAP) kinase 2 suggests a bifunctional switch that couples kinase activation with nuclear export. J. Biol. Chem. *277*, 37401–37405.

Muniyappa, H., and Das, K.C. (2008). Activation of c-Jun N-terminal kinase (JNK) by widely used specific p38 MAPK inhibitors SB202190 and SB203580: A MLK-3-MKK7-dependent mechanism. Cell. Signal. *20*, 675–683.

Nardozzi, J.D., Lott, K., and Cingolani, G. (2010). Phosphorylation meets nuclear import: a review. Cell Commun. Signal. *8*, 32.

Ninomiya-Tsuji, J., Kishimoto, K., Hiyama, A., Inoue, J., Cao, Z., and Matsumoto, K. (1999). The kinase TAK1 can activate the NIK-I kappaB as well as the MAP kinase cascade in the IL-1 signalling pathway. Nature *398*, 252–256.

Niwa, H., Yamamura, K., and Miyazaki, J. (1991). Efficient selection for high-expression transfectants with a novel eukaryotic vector. Gene *108*, 193–199.

Noguchi, K., Kitanaka, C., Yamana, H., Kokubu, A., Mochizuki, T., and Kuchino, Y. (1999). Regulation of c-Myc through phosphorylation at Ser-62 and Ser-71 by c-Jun N-terminal kinase. J. Biol. Chem. *274*, 32580–32587.

Ono, K., and Han, J. (2000). The p38 signal transduction pathway: activation and function. Cell. Signal. *12*, 1–13.

Paek, A.L., Liu, J.C., Forrester, W.C., Lahav, G., Paek, A.L., Liu, J.C., Loewer, A., Forrester, W.C., and Lahav, G. (2016). Cell-to-Cell Variation in p53 Dynamics Leads to Fractional Killing. Cell *165*, 1–12.

Perdiguero, E., Ruiz-Bonilla, V., Gresh, L., Hui, L., Ballestar, E., Sousa-Victor, P., Baeza-Raja, B., Jardi, M., Bosch-Comas, A., Esteller, M., et al. (2007). Genetic analysis of p38 MAP kinases in myogenesis: fundamental role of p38alpha in abrogating myoblast proliferation. EMBO J. *26*, 1245–1256.

Pereira, L., Igea, A., Canovas, B., Dolado, I., and Nebreda, A.R. (2013). Inhibition of p38 MAPK sensitizes tumour cells to cisplatin-induced apoptosis mediated by reactive oxygen species and JNK. EMBO Mol. Med. *5*, 1759–1774.

Purvis, J.E., and Lahav, G. (2013). Encoding and decoding cellular information through signaling dynamics. Cell *152*, 945–956.

Purvis, J.E., Karhohs, K.W., Mock, C., Batchelor, E., Loewer, A., and Lahav, G. (2012). p53

dynamics control cell fate. Science *336*, 1440–1444.

Raingeaud, J., Gupta, S., Rogers, J.S., Dickens, M., Han, J., Ulevitch, R.J., and Davis, R.J. (1995). Pro-inflammatory cytokines and environmental stress cause p38 mitogen-activated protein kinase activation by dual phosphorylation on tyrosine and threonine. J. Biol. Chem. *270*, 7420–7426.

Raingeaud, J., Whitmarsh, A.J., Barrett, T., Dérijard, B., Davis, R.J., Raingeaud, L., Whitmarsh, A.J., Barrett, T., De, B., and Davis, R.J. (1996). MKK3- and MKK6-regulated gene expression is mediated by the p38 mitogen-activated protein kinase signal transduction pathway. Mol. Cell. Biol. *16*, 1247–1255.

Raman, M., Chen, W., and Cobb, M.H. (2007). Differential regulation and properties of MAPKs. Oncogene *26*, 3100–3112.

Ran, F.A., Hsu, P.D., Wright, J., Agarwala, V., Scott, D.A., and Zhang, F. (2013). Genome engineering using the CRISPR-Cas9 system. Nat. Protoc. *8*, 2281–2308.

Regot, S., Hughey, J.J., Bajar, B.T., Carrasco, S., and Covert, M.W. (2014). High-sensitivity measurements of multiple kinase activities in live single cells. Cell *157*, 1724–1734.

Rouse, J., Cohen, P., Trigon, S., Morange, M., Alonso-Llamazares, A., Zamanillo, D., Hunt, T., and Nebreda, A.R. (1994). A novel kinase cascade triggered by stress and heat shock that stimulates MAPKAP kinase-2 and phosphorylation of the small heat shock proteins. Cell *78*, 1027–1037.

Roux, J., Hafner, M., Bandara, S., Sims, J.J., Hudson, H., Chai, D., and Sorger, P.K. (2015). Fractional killing arises from cell-to-cell variability in overcoming a caspase activity threshold. Mol. Syst. Biol. *11*, 1–18.

Sanjana, N.E., Shalem, O., and Zhang, F. (2014). Improved vectors and genome-wide libraries for CRISPR screening. Nat. Methods *11*, 783–784.

Santos, S.D.M., Verveer, P.J., and Bastiaens, P.I.H. (2007). Growth factor-induced MAPK network topology shapes Erk response determining PC-12 cell fate. Nat. Cell Biol. *9*, 324–330.

Schmittgen, T.D., and Livak, K.J. (2008). Analyzing real-time PCR data by the comparative CT method. Nat. Protoc. *3*, 1101–1108.

Shibuya, H., Yamaguchi, K., Shirakabe, K., Tonegawa, A., Gotoh, Y., Ueno, N., Irie, K., Nishida, E., and Matsumoto, K. (1996). TAB1: an activator of the TAK1 MAPKKK in TGF-β signal transduction. Science *272*, 1179–1182.

Slack, D.N., Seternes, O.M., Gabrielsen, M., and Keyse, S.M. (2001). Distinct binding determinants for ERK2/p38alpha and JNK map kinases mediate catalytic activation and substrate selectivity of map kinase phosphatase-1. J. Biol. Chem. *276*, 16491–16500.

Spencer, S.L., Gaudet, S., Albeck, J.G., Burke, J.M., and Sorger, P.K. (2009). Non-genetic origins of cell-to-cell variability in TRAIL-induced apoptosis. Nature *459*, 428–432.

Staples, C.J., Owens, D.M., Maier, J.V., Cato, A.C.B., and Keyse, S.M. (2010). Cross-talk

between the p38α and JNK MAPK pathways mediated by MAP kinase phosphatase-1 determines cellular sensitivity to UV radiation. J. Biol. Chem. *285*, 25928–25940.

Thornton, T.M., and Rincon, M. (2009). Non-classical p38 map kinase functions: cell cycle checkpoints and survival. Int. J. Biol. Sci. *5*, 44–51.

Tomida, T., Takekawa, M., and Saito, H. (2015). Oscillation of p38 activity controls efficient pro-inflammatory gene expression. Nat. Commun. *6*, 8350.

Tournier, C., Hess, P., Yang, D.D., Xu, J., Turner, T.K., Nimnual, A., Bar-Sagi, D., Jones, S.N., Flavell, R.A., and Davis, R.J. (2000). Requirement of JNK for stress-induced activation of the cytochrome c-mediated death pathway. Science *288*, 870–874.

Trask, O.J., Baker, A., Williams, R.G., Nickischer, D., Kandasamy, R., Laethem, C., Johnston, P.A., and Johnston, P.A. (2006). Assay Development and Case History of a 32K-Biased Library High-Content MK2-EGFP Translocation Screen to Identify p38 Mitogen-Activated Protein Kinase Inhibitors on the ArrayScan 3.1 Imaging Platform. Methods Enzymol. *414*, 419–439.

Wagner, E.F., and Nebreda, Á.R. (2009). Signal integration by JNK and p38 MAPK pathways in cancer development. Nat. Rev. Cancer *9*, 537–549.

Wakamoto, Y., Dhar, N., Chait, R., Schneider, K., Signorino-Gelo, F., Leibler, S., McKinney, J.D., and Chemistry, T. (2013). Dynamic Persistence of Antibiotic-Stressed Mycobacteria. Science *339*, 91–95.

Waskiewicz, A.J., Flynn, A., Proud, C.G., and Cooper, J.A. (1997). Mitogen-activated protein kinases activate the serine/threonine kinases Mnk1 and Mnk2. EMBO J. *16*, 1909–1920.

Werner, S.L., Barken, D., and Hoffmann, A. (2005). Stimulus specificity of gene expression programs determined by temporal control of IKK activity. Science *309*, 1857–1861.

Weston, C.R., and Davis, R.J. (2007). The JNK signal transduction pathway. Curr. Opin. Cell Biol. *19*, 142–149.

Whitmarsh, A.J., Shore, P., Sharrocks, A.D., and Davis, R.J. (1995). Integration of MAP kinase signal transduction pathways at the serum response element. Science *269*, 403–407.

Yamamoto, K., Ichijo, H., and Korsmeyer, S.J. (1999). BCL-2 is phosphorylated and inactivated by an ASK1/Jun N-terminal protein kinase pathway normally activated at G(2)/M. Mol. Cell. Biol. *19*, 8469–8478.

Yoshida, K., Yamaguchi, T., Natsume, T., Kufe, D., and Miki, Y. (2005). JNK phosphorylation of 14-3-3 proteins regulates nuclear targeting of c-Abl in the apoptotic response to DNA damage. Nat. Cell Biol. *7*, 278–285.

Yusa, K., Rad, R., Takeda, J., and Bradley, A. (2009). Generation of transgene-free induced pluripotent mouse stem cells by the piggyBac transposon. Nat. Methods *6*, 363–369.

Zhao, M., New, L., Kravchenko, V.V., Kato, Y., Gram, H., di Padova, F., Olson, E.N., Ulevitch, R.J., and Han, J. (1999). Regulation of the MEF2 family of transcription factors by

p38. Mol. Cell. Biol. *19*, 21–30.

Zhao, Q., Wang, X., Nelin, L.D., Yao, Y., Matta, R., Manson, M.E., Baliga, R.S., Meng, X., Smith, C.V., Bauer, J.A., et al. (2006). MAP kinase phosphatase 1 controls innate immune responses and suppresses endotoxic shock. J. Exp. Med. *203*, 131–140.

Acknowledgments

Firstly, I would like to express my sincere gratitude to my supervisors Prof. Kazuhiro Aoki and Prof. Michiyuki Matsuda for their continuous support of my doctoral study. Their scientific guidance, valuable discussions, and immense knowledge helped me in all the time of research, leading to this thesis. I want to thank Prof. Kazuhiro Aoki for his encouragement to pursue science, mentorship with the right balance of freedom and guidance, and providing a healthy, happy, and safe lab environment on a daily basis. I am also very grateful to Assis. Prof. Yohei Kondo for his support in statistical analysis and contributions to my thesis work.

I want to thank all the members of Aoki lab. Thanks to Dr. Shigekazu Oda, Dr. Yuhei Goto, Dr. Reina Itoh, Dr. Akira Komatsubara, Youichi Uda, Gembu Maryu, Ryosuke Tanii, and Masaya Mukai for their discussions, advice, help, kindness, and all the enjoyable moments we had the past years. Special thanks to Emi Ebine, Kaori Onoda, Naoko Nishimoto, Kyoko Hirano, Akiko Kawagishi, and Nobuyo Sakikawa for their precious technical support and motivation. I am thankful to my numerous colleagues at Matsuda lab for all the insightful discussions and advice. I also thank my friends at Kyoto University and National Institutes of Natural Sciences. In particular, I am grateful to Dr. Yousef Yari Kamrani for priceless discussions, critical reading of my manuscript, encouragement, and support. I also want to acknowledge Kyoto University Graduate School of Biostudies, the National Institute for Basic Biology, and Japanese Society for Promotion of Science for providing an excellent research environment and financial means to complete my studies.

Last but not least, I would like to thank my family, my parents and my sister, for their motivation and support during my PhD work.

This thesis is based on material contained in the following scholarly paper:
Haruko Miura, Yohei Kondo, Michyuki Matsuda, Kazuhiro Aoki.
Cell-to-Cell Heterogeneity in p38-Mediated Cross-Inhibition of JNK Causes Stochastic Cell Death.
Cell Reports, Volume 24, Issue 10, Pages 2658-2668, September 2018